รายงานวิจัยฉบับสมบูรณ์

โครงการการศึกษาคุณสมบัติทางโครงสร้างและโมเลกุลของ levan oligosaccharides ที่มีความยาวที่แตกต่างกัน

โดย ดร.สุรศักดิ์ ชื่นศรีวิโรจน์

มิถุนายน 2560

สัญญาเลขที่ TRG5880222

รายงานวิจัยฉบับสมบูรณ์

โครงการการศึกษาคุณสมบัติทางโครงสร้างและโมเลกุลของ levan oligosaccharides ที่มีความยาวที่แตกต่างกัน

ดร.สุรศักดิ์ ชื่นศรีวิโรจน์
ภาควิชาชีวเคมี คณะวิทยาศาสตร์ จุฬาลงกรณ์มหาวิทยาลัย

สนับสนุนโดยสำนักงานกองทุนสนับสนุนการวิจัยและ
จุฬาลงกรณ์มหาวิทยาลัย

Abstract

Project Code : TRG5880222

Project Title : Elucidation of the structural and molecular properties of levan oligosaccharides of various chain lengths

Investigators : Pongsakorn Kanjanatanin, Assistant Prof. Dr. Rath Pichayangkura and Dr. Surasak Chunsrivirot*

Department of Biochemistry, Faculty of Science, Chulalongkorn University

E-mail Address : surasak.ch@chula.ac.th*

Project Period : July 2015 – June 2017

Levan and levan-type fructo-oligosaccharides (LFOs) have various potential applications in pharmaceutical and food industries due to their beneficial properties such as their low intrinsic viscosity and high water solubility. Previous studies showed that they exhibited prebiotic effects, anti-inflammatory and anti-tumor activities against Sarcoma-180 tumor cells of human. Despite their various potential applications, the structural and molecular properties of LFOs of various chain lengths are not well understood. In this study, we employed the replica-exchange molecular dynamics simulations method (REMD) in AMBER14 to elucidate structural and molecular properties of LFOs with chain lengths of 5 (LFO_5), 10 (LFO_{10}) and 15 (LFO_{15}) residues in two models of generalized Born implicit solvent (GB_{HCT} and GB_{OBC1}). For LFO_{10} and LFO_{15}, four distinct conformations (helix-like, partial helix, zig-zag and random structures) were characterized by their upper-middle and lower-middle torsions. For LFO_5, two distinct conformations (partial helix and random structures) were characterized by their middle torsion and molecular angle of residues 1, 3 and 5. To determine hydrogen bonds important for the formation of helix-like structures of LFO_{10} and LFO_{15}, occurrence frequencies of hydrogen bonds were analyzed, and the $O6_{(i)}$--$H3O_{(i+1)}$ hydrogen bond was found with the highest frequency, suggesting its importance in helix formation. Among three dihedral angles between two fructosyl units [ϕ (O5'-C2'-O6-C6), ψ (C2'-O6-C6-C5) and ω (O6-C6-C5-C4)], dihedral angle distributions showed that ω was the most flexible dihedral angle and probably responsible for conformational differences of LFOs. Our study provides important insights into the structural and molecular properties of LFOs, which tend to form helical structures as the chain length increases from 5 to 15 residues. This information could be beneficial for the selection of LFOs with appropriate lengths and properties for pharmaceutical and biological application.

Keywords : levan, oligosaccharide, helix, replica exchange molecular dynamics simulations

บทคัดย่อ

รหัสโครงการ: TRG5880222

ชื่อโครงการ : การศึกษาคุณสมบัติทางโครงสร้างและโมเลกุลของ levan oligosaccharides ที่มีความยาวที่แตกต่างกัน

ชื่อนักวิจัย : นายพงศกร กาญจนธานินทร์, ผศ.ดร. รัฐ พิชญางกูร และ ดร.สุรศักดิ์ ชื่นศรีวิโรจน์*

ภาควิชาชีวเคมี คณะวิทยาศาสตร์ จุฬาลงกรณ์มหาวิทยาลัย

E-mail Address : surasak.ch@chula.ac.th*

ระยะเวลาโครงการ : ก.ค. 2558 – มิ.ย. 2560

levan และ levan oligosaccharides (LFOs) มีศักยภาพที่จะนำไปประยุกต์ใช้ทางด้านอุตสาหกรรมยาและอาหารเนื่องจาก levan และ LFOs มีคุณสมบัติที่เป็นประโยชน์ เช่น มีความหนืดที่ต่ำและสามารถละลายน้ำได้ดี การศึกษาก่อนหน้านี้แสดงให้เห็นว่า levan และ LFOs แสดงความเป็นพรีไบโอติก มีความสามารถในการต่อต้านการอักเสบและต่อต้านเนื้องอกในมนุษย์ชนิด Sarcoma-180 ถึงแม้ว่า levan และ LFOs จะมีศักยภาพในการนำไปประยุกต์ใช้อย่างหลากหลาย ความเข้าใจในสมบัติทางโครงสร้างและโมเลกุลของ LFOs ยังมีอยู่อย่างจำกัด ในการศึกษานี้ได้ใช้วิธี replica-exchange molecular dynamics simulations method (REMD)โดยใช้โปรแกรม AMBER14 เพื่ออธิบายสมบัติทางโครงสร้างและโมเลกุลของ LFOs ที่มีความยาว 5 (LFO_5), 10 (LFO_{10}) และ 15 (LFO_{15}) หน่วย ใน generalized Born implicit solvent 2 โมเดล (GB_{HCT} และ GB_{OBC1}) สำหรับ LFO_{10} และ LFO_{15} นั้นพบว่ามี 4 conformations (โครงสร้างแบบ helix-like, partial helix, zig-zag และ random) เมื่อใช้ upper-middle และ lower-middle torsions มาอธิบายลักษณะ สำหรับ LFO_5 นั้นพบว่ามี 2 conformations (โครงสร้างแบบ partial helix และ random) เมื่อใช้ middle torsion และ molecular angle ของ residue 1 3 และ 5 มาอธิบายลักษณะ ความถี่ของการเกิดพันธะไฮโดรเจนถูกนำมาใช้เพื่อศึกษาพันธะไฮโดรเจนที่มีความสำคัญต่อการเกิดโครงสร้างแบบ helix และพบว่าพันธะไฮโดรเจน $O6_{(i)}$--$H3O_{(i+1)}$ มีความถี่สูงสุดซึ่งพันธะนี้น่าจะมีความสำคัญต่อการเกิด helix สำหรับ dihedral angle 3 มุมระหว่าง fructosyl residue 2 หน่วย [ϕ (O5'-C2'-O6-C6), ψ (C2'-O6-C6-C5) and ω (O6-C6-C5-C4)] นั้น การกระจายตัวของ dihedral angle แสดงให้เห็นว่า ω เป็นมุมที่มีความยืดหยุ่นที่สุด และน่าจะเป็นมุมที่ทำให้โครงสร้างของ LFO มีความแตกต่างกัน การศึกษานี้ได้ให้ความรู้ที่สำคัญเกี่ยวกับสมบัติทางโครงสร้างและโมเลกุลของ LFOs ซึ่งมีแนวโน้มจะมีโครงสร้างเป็นแบบ helix เมื่อความยาวเพิ่มขึ้นจาก 5 เป็น 15 หน่วย ความรู้ที่ได้จากงานนี้น่าจะเป็นประโยชน์ในการนำมาใช้เลือก LFOs ที่มีความยาวและคุณสมบัติที่เหมาะสมสำหรับการนำไปประยุกต์ใช้ทางด้านเภสัชกรรมและชีวภาพ

คำหลัก : levan, oligosaccharide, helix, replica exchange molecular dynamics simulations

Introduction

As a microbial polyfructan, levan consists of D-fructofuranosyl residues predominantly linked by β-(2, 6) linkage in a main chain with some β-(2, 1) linked branching points (Fig. 1). It is produced by levansucrase in various organisms that were grown in sucrose-containing medium. Levansucrase is a member of glycoside hydrolase family 68 that catalyzes a transfructosylation reaction to grow the levan chain, and also catalyzes a sucrose hydrolysis into glucose and fructose. Levansucrase is predominantly detected in bacteria such as *Bacillus subtilis* (*1*), *Z. mobilis* (*2*), *Gluconacetobacter diazotrophicus* (*3*), *Pseudomonas syringae pv. Phaseolicola* (*4*), *Rahnella aquatilis* (*5*), and *Leuconostoc mesenteroides* (*6*).

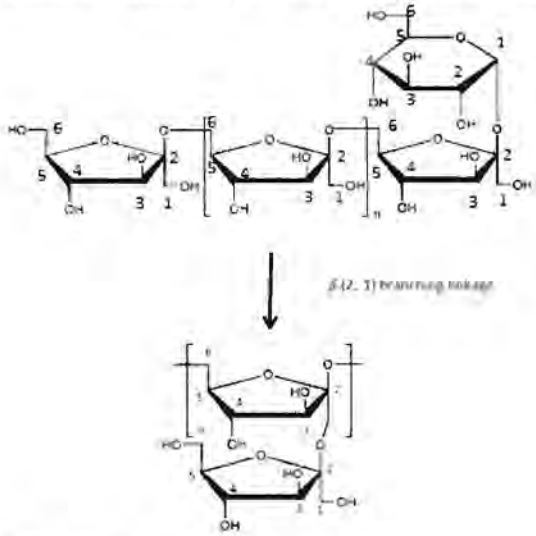

Fig 1. Levan structure.

Levan and LFOs have various desirable properties such as their unusually low intrinsic viscosity (*7*), high water solubility and susceptibility to acid hydrolysis (*8*). These properties are very beneficial for various industrial applications, especially in food and pharmaceutical industries. In food industry, levan and LFOs can potentially be used as cholesterol- and triacylglycerol-lowering agents (*9*) and prebiotics (*10*). In pharmaceutical industry, they have potential to be used as binders, controlled-release matrices (*11*), antiviral agents against avian influenza HPAI, H5N1 and adenovirus type 40 (*12*) as well as antitumor agents, whose activities depend on the chain lengths and degrees of branching of levan (*13, 14*). In addition, they could be developed for use as environmentally friendly adhesives, water resistant films for food preservation and for shale stabilization in the oil drilling industry because of its film-forming ability, non-toxicity and adhesive strength that are comparable to petrochemical derivatives (*15*). They could also be used as cryoprotectants for freeze-preservation of fish, animal cells and the delicate texture of frozen desserts (*16*).

Molecular dynamics (MD) simulations technique is employed to describe time-dependent atomic motions of a system. This technique integrates Newton's equations of motion, using inter-atomic forces generated from the potential energy of the system. Some molecular dynamics studies have been carried out to investigate the properties of oligosaccharides in solution. For example, Franca *et al.* performed simulations of chitosan single chains and chitin nanoparticle aggregates with varied percentages and distributions of acetyl groups (*17, 18*). They found that after 40ns simulations chitin was in an aggregate form (insoluble), whereas chitosan chains were separated and fully hydrated. Their results showed that chitosan conformation and solubility were strongly dependent on pH and degree of acetylation. Moreover, they found that the loss of flexibility and conformational interchangeability seemed to be caused by the increase in acetylation level (*19*). MD technique has also been used to investigate the effects of chemical modifications of the glycans (*20*), conformations of N-linked glycans that underpin inflammation and immunity (21), and the structures and dynamics of β-l-Fuc*p*-(1⟶6)-α-d-Glc*p*-OMe (*22*), lipopolysaccharide (*23*) and lipid-linked oligosaccharide in membrane bilayers.

To achieve good samplings, REMD simulates a number of replicas of the system at different temperatures and exchanges the non-interacting systems among them. Although low temperature simulations allow precise sampling in a local region of phase space, the system can be trapped in a local minimum during the time scale of the normal simulation method as they cannot overcome an energy barrier. Raising the temperature can increase the probability of the system to overcome the energy barrier, consequently enhancing the probability of attaining the global minimum and allowing the sampling of large volumes of phase space. Therefore, the incorporation of higher temperature systems allow the lower temperature systems to access a representative set of the low free energy minima that are accessible by the higher temperature systems (*24*). The replica exchange technique has been use in various studies such as the investigations of the conformational flexibility of soluble cellulose oligomers (*25*), the effects of bisecting GlcNAc and core fucosylation on conformational properties of biantennary complex-type N-glycans in solution (*26*), and the structural diversity and changes in conformational equilibria of biantennary complex-type N-glycans in water (*27*). However, since this method requires the simulations of various replicas at different temperatures at once, it is computationally expensive, time-consuming and resource-consuming, especially in explicit solvent simulatins, where water molecules are explicitly represented in the systems. To circumvent this problem to some extend, some research

studies used implicit solvent model, where the properties of water molecules and their interactions are incorporated into the energy function directly (*28*), sacrificing the accuracy of using explicit water molecules in the simulations. An example of the studies employing this approach is the work done by Rungnim, C, et al., where they used replica exchange method with implicit solvent models to investigate the effects of chitosan chain lengths on the molecular properties and dynamic behaviors of targeted drug delilvery system (*29*).

Although LFOs have various potential applications, the structural and molecular properties of LFOs of various chain lengths are not well-understood. The aims of this study are to build possible models of LFOs with various chain lengths in solution and to elucidate their structural and molecular properties as well as the relationships between the properties and the chain length. Two molecular simulations techniques (MD and REMD) will be performed on these systems. REMD simulates a system at various temperatures at once, and exchanges the non-interacting systems among them and therefore could enhance the sampling accuracy. However, this method is computationally expensive, time-consuming and resource-consuming, as compared to MD that simulates a system at one temperature. Therefore, MD will be initially used in a preliminary study. The knowledge on the structural and molecular properties of LFOs gained from this study would be beneficial in selecting LFOs with appropriate chain lengths and properties for their potential applications. Moreover, the constructed models of LFOs could also be used for future computational studies.

Objectives

- To construct possible models of LFOs of various chain lengths.
- To elucidate the structural and molecular properties of LFOs of various chain lengths in solution, and the relationships between the properties and the chain length.

Methods

MD of LFOs in explicit solvent model (preliminary study)

Structure preparation and minimization

The structures of LFO_5, LFO_{10} and LFO_{15} (Fig. 2) were constructed using the LEaP module in AMBER14 (*30*), and their atom types and force field parameters were assigned based on GLYCAM06j-1 (*31*). All systems were solvated in truncated octahedral TIP3P water box with the size of 10 Å. AMBER14 software with the non-bonded cutoff of 9 Å was used for all systems in the minimizations and simulations. Using restraints with the force constant of 10.0 kcal/(mol $Å^2$) on solute atoms, all systems were minimized with 2,500 steepest-descent minimization cycles and 2,500 conjugate-gradient minimization cycles (*32, 33*). With no restraint, they were further minimized with 2,500 steepest-descent minimization cycles and 2,500 conjugate-gradient minimization cycles.

MD

All bond-stretching freedoms associated with hydrogen were eliminated by SHAKE algorithm, allowing a time step of 0.002 ps (*35*). Applying restraints with the force constant of 10.0 kcal/(mol $Å^2$) on solute atoms, all systems were heated to 298K for 50 ps in the NVT ensemble. They were further equilibrated at 298K for 100 ps in the NVT ensemble. In the NPT ensemble, they were then simulated at 298K and 1 atm for 30 ns and their trajectories were used for further analyses.

REMD of LFOs in GB_{OBC1} and GB_{HCT} implicit solvent models

Structure preparation and minimization

The structures of LFO_5, LFO_{10} and LFO_{15} were constructed (Fig. 2) using the LEaP module in AMBER14, and their atom types and force field parameters were assigned based on GLYCAM06j-1. Two implicit solvent models (GB_{HCT} and GB_{OBC1}) were used in the minimization and simulations of each system. All systems were minimized with 2,500 steepest-descent minimization cycles and 2,500 conjugate-gradient minimization cycles.

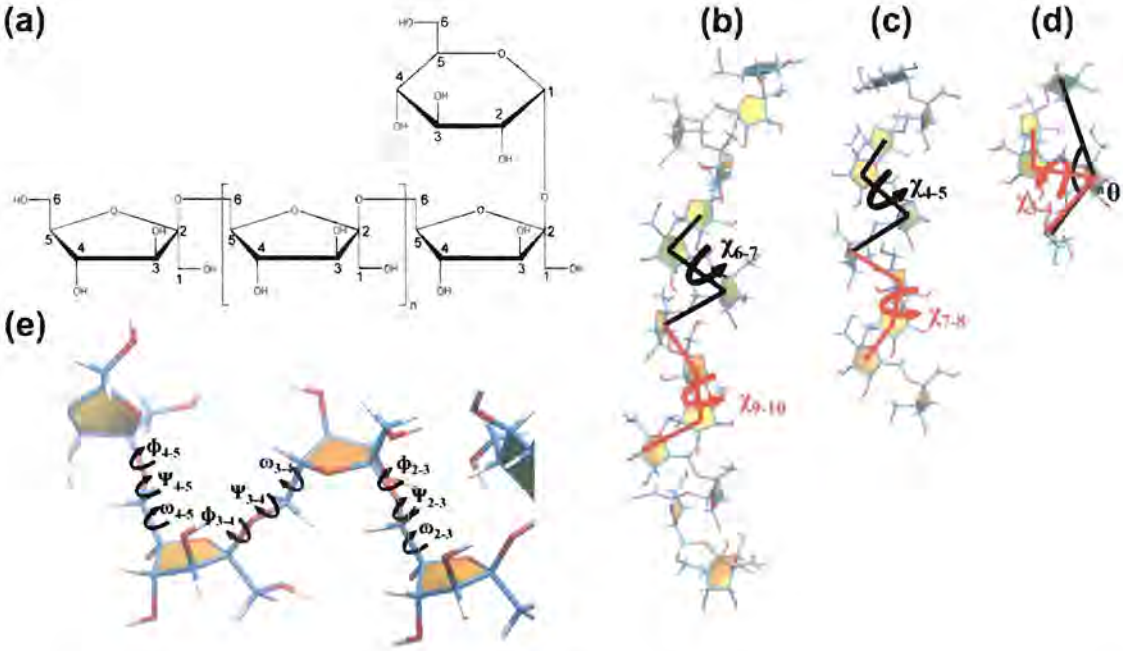

Fig 2. (a) An example of LFO structure with no branch. (b) The parameters used in the characterization of the conformations of LFOs: the upper-middle ($\chi_{6\text{-}7}$) and lower-middle ($\chi_{9\text{-}10}$) torsions for LFO_{15}, (c) the upper-middle ($\chi_{3\text{-}4}$) and lower-middle ($\chi_{7\text{-}8}$) torsions for LFO_{10}, (d) the molecular angles (θ_a) and middle torsions ($\chi_{3\text{-}4}$) for LFO_5. (e) Examples of three dihedral angles between four fructosyl residues of LFO_5, ω (C4-C5-C6-O6), ψ (C5-C6-O6-C2') and ϕ (C6-O6-C2'-O5'). The carbon, oxygen and hydrogen atoms were colored in green, red and white, respectively. The six-membered ring of the glucosyl residue and the five-membered rings of fructosyl residue are shown in green and yellow, respectively.

Replica exchange molecular dynamics simulations

Sixteen replicas of each system were initially equilibrated for 500 ps to reach the desired temperature range from 262 K to 802 K. REMD of all systems were performed using the SANDER module in AMBER14. Langevin dynamics with a collision frequency of 1 ps^{-1} were used to control the temperatures in all systems. Initial velocity of each system was reseeded by the random number generator (*34*). A cut off of 999 Å was used to truncate nonbonded pairs, and the maximum distance of 999 Å between atom pairs was employed to compute the pairwise summation involved in the effective Born radii calculation. All bond-stretching freedoms associated with hydrogen were eliminated by SHAKE algorithm, allowing a time step of 0.002 ps. Each replica was simulated for 100 ns and exchanged every 2 ps. The replicas at 298 K were employed for the analyses of the structural and molecular properties of LFOs with different chain lengths.

To measure the sizes of all systems, their average radii of gyration (ROG) were determined.

To determine possible representative structures of LFOs of each chain length, K-means clustering algorithm, as implemented in MMTSB tool sets (*36*), was employed to cluster the structures from their 100 ns trajectories based on their structural similarities, calculated from their heavy-atom root-mean-square-deviation. To determine a reasonable representative of each cluster, a structure that is most similar to the average structure of all members of each cluster was chosen to be a "centroid;" i.e., a "centroid" is a structure with the lowest heavy-atom root-mean-square-deviation to the average structure. Based on their shapes, these "centroids" were further classified into helix-like, partial helix, zig-zag or random structures as major representative conformers. Helix-like structures were defined as conformations that had more than one helical turn, while partial helix structures were defined as conformations that had one helical turn. Zig-zag structures were defined as conformations that had zig-zag shapes. Random structures were defined as structures that were not classified as helix-like, partial helix or zig-zag structures.

To plot the free energy map, various parameters were employed to characterize the structures of LFOs. Since helix-like conformations were observed with high frequency in LFO_{10} and LFO_{15} and they tended to have similar values of upper-middle and lower-middle torsions, their upper-middle and lower-middle torsions were used to characterize the structures of LFO_{10} and LFO_{15}. Their upper-middle torsions were computed by measuring the torsion angles of the centers of masses (CM) of residues 5, 6, 7 and 8 (defined as $\chi_{6\text{-}7} = CM_5\text{-}CM_6\text{-}CM_7\text{-}CM_8$) and residues 3, 4, 5 and 6 (defined as $\chi_{4\text{-}5} = CM_3\text{-}CM_4\text{-}CM_5\text{-}CM_6$) for LFO_{15} and LFO_{10}, respectively. Their lower-middle torsions were computed by measuring the torsion angles of the centers of masses (CM) of residues 8, 9, 10 and 11 (defined as $\chi_{9\text{-}10} = CM_8\text{-}CM_9\text{-}CM_{10}\text{-}CM_{11}$) and residues 6, 7, 8 and 9 (defined as $\chi_{7\text{-}8} = CM_6\text{-}CM_7\text{-}CM_8\text{-}CM_9$) for LFO_{15} and LFO_{10}, respectively (Fig. 2(b, c)). For LFO_5, the molecular angles and middle torsions were computed by measuring the angles and torsion angles of the centers of masses (CM) of residues 1, 3 and 5 (defined as $\theta_a = CM_1\text{-}CM_3\text{-}CM_5$) and residues 2, 3, 4 and 5 (defined as $\chi_{3\text{-}4} = CM_2\text{-}CM_3\text{-}CM_4\text{-}CM_5$), respectively (Fig. 2(d)).

To measure conformational flexibilities, the occurrence frequencies of three dihedral angles between every two fructosyl residues, ω (C4-C5-C6-O6), ψ (C5-C6-O6-C2') and ϕ (C6-O6-C2'-O5') (Fig. 2(e)) were computed. To identify hydrogen bonds important for the formation of helix-like structures of LFO_{10} and LFO_{15}, the occurrence

frequencies of hydrogen bonds were measured. Only the hydrogen bonds with the occurrence frequency of at least 1 percent were used for further analysis.

Results and discussion

MD of LFOs in explicit solvent (preliminary study)

As a preliminary study, we applied MD technique on LFO_5, LFO_{10} and LFO_{15} because it uses less time and resources than REMD although its results may be less accurate than those of REMD. The final structures after 30 ns simulations are shown in Table 1.

Table 1. The initial and final structures of LFO_5, LFO_{10} and LFO_{15} after 30 ns MD.

	chain length		
	5	10	15
before MD			
after MD			

After MD, the structures were significantly different from the initial structures. Various structures were found such as random coils, helix-like structures or combinations of different structures.

Sizes of LFOs

The sizes of LFOs were approximated by their radii of gyration. The relationship between the radius of gyration and the length of LFOs is shown in Fig. 3.

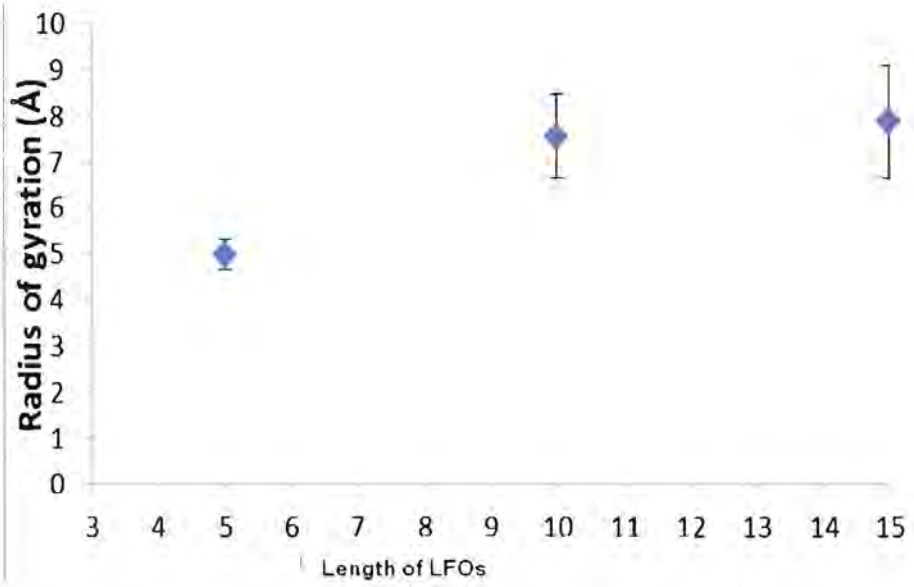

Fig 3. The relationship between radius of gyration and the length of LFOs.

As the chain lengths of LFOs increases, their radii of gyration increase, indicating the extension of their sizes.

Structural clustering

Employing K-mean clustering algorithm, MMTSB software was employed to cluster the structures of LFOs based on their structural similarities as measured by their RMSD values. Structures were classified into the same group if their RMSD values were within a specified cutoff RMSD value from the centroid. To find an appropriate cutoff for structural clustering, a cutoff of 4 Å was initially used. This cutoff was increased by 0.5 Å until each group could be appropriately classified. Then the structure most similar to the centroid of each group was superimposed to compute the RMSD value. The criteria for cutoff value selection were that the number of groups should be less than or equal to four and its RMSD value divided by its chain length should be more than 0.46.

Table 2 shows the appropriate cutoff value for structural clustering of each chain length. The results suggested that the appropriate cutoff values for LFO_5, LFO_{10} and LFO_{15} were 4, 5 and 7 Å, respectively. Using these criteria, the structures of LFOs were categorized into about two to three groups.

Table 2 Cut off values and number of groups obtained from structural clustering.

chain length	cut off (Å)	number of group
5	4	3
10	5	2
15	7	3

Representative structures most similar to the centroid of each group of LFO_5, LFO_{10} and LFO_{15} are shown in Table 3. The structures of LFO_5 were characterized into three groups: partial helix (53.2%), random coil (39.5%) and linear (7.2%). The structures of LFO_{10} were classified into two groups: extended helix (77.0%) and helix (23.0%). The structures of LFO_{15} were categorized into three groups: random coil (70.7%), relaxed random coil (19.3%) and extended random coil (10.0%).

Table 3 Representative structures from each group of LFO_5, LFO_{10} and LFO_{15} and their populations.

chain length	representative structure most similar to the centroid of the group	population
5	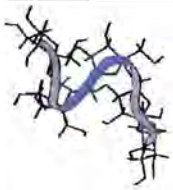 partial helix	53.2%
	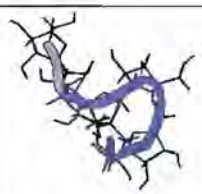 random coil	39.5%
	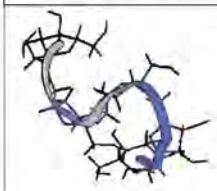 Linear	7.2%

10	 extended helix	77.0%
	 Helix	23.0%
15	 random coil	70.7%
	 relaxed random coil	19.3%
	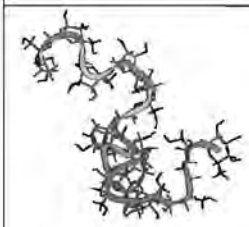 extended random coil	10.0%

REMD of LFOs in GB_{OBC1} and GB_{HCT} implicit solvent models

Although MD requires less time and resources than REMD, MD may not be able to sample the most possible and accurate structures that can be found in nature because the systems sampled by MD at low temperature cannot overcome an energy barrier and can get trapped in a local minimum. REMD simulates a number of replicas of the system at different temperatures and exchanges the non-interacting systems among them. Raising the temperature can increase the probability of the system to overcome the energy barrier, consequently enhancing the probability of attaining the global minimum and allowing the sampling of large volumes of phase space. As a result, the incorporation of higher temperature systems allow the lower temperature systems to access a representative set of the low free energy minima that are accessible by the higher temperature systems. Therefore, REMD was employed to simulate the systems of LFO_5, LFO_{10} and LFO_{15} at 16 temperatures to improve the accuracy of the results. However, since REMD is very computationally expensive, two implicit solvent models, i.e., GB_{OBC1} and GB_{HCT} were employed instead of explicit solvent model.

Reliability of REMD simulations.

To determine whether the temperatures were optimally distributed and the number of replicas was sufficient, the acceptance ratios of replica exchange were calculated. The acceptance ratios of the simulations of LFO_{15} in the GB_{HCT} model were almost constant around 28%, implying a free random walk in the replica (temperature) space (Fig. 4(a)). Moreover, a free random walk both in the replica space (Fig. 4(b)) and the temperature space (Fig. 4(c)) were also confirmed. Furthermore, the canonical probability distribution of the total potential energy at each temperature had sufficient overlap with those of neighbors (Fig. 4(d)). The results of the REMD simulations of LFO_{10} and LFO_5 in the GB_{HCT} model were also similar, and their average acceptance ratios were almost constant around 37% and 50% for LFO_{10} and LFO_5, respectively. For the systems simulated in the GB_{OBC1} model, the results of REMD simulations were also similar to those simulated in the GB_{HCT} model, and their average acceptance ratios were almost constant around 28%, 36% and 50% for LFO_{15}, LFO_{10} and LFO_5, respectively. These results indicate good reliability of the REMD simulations of all systems.

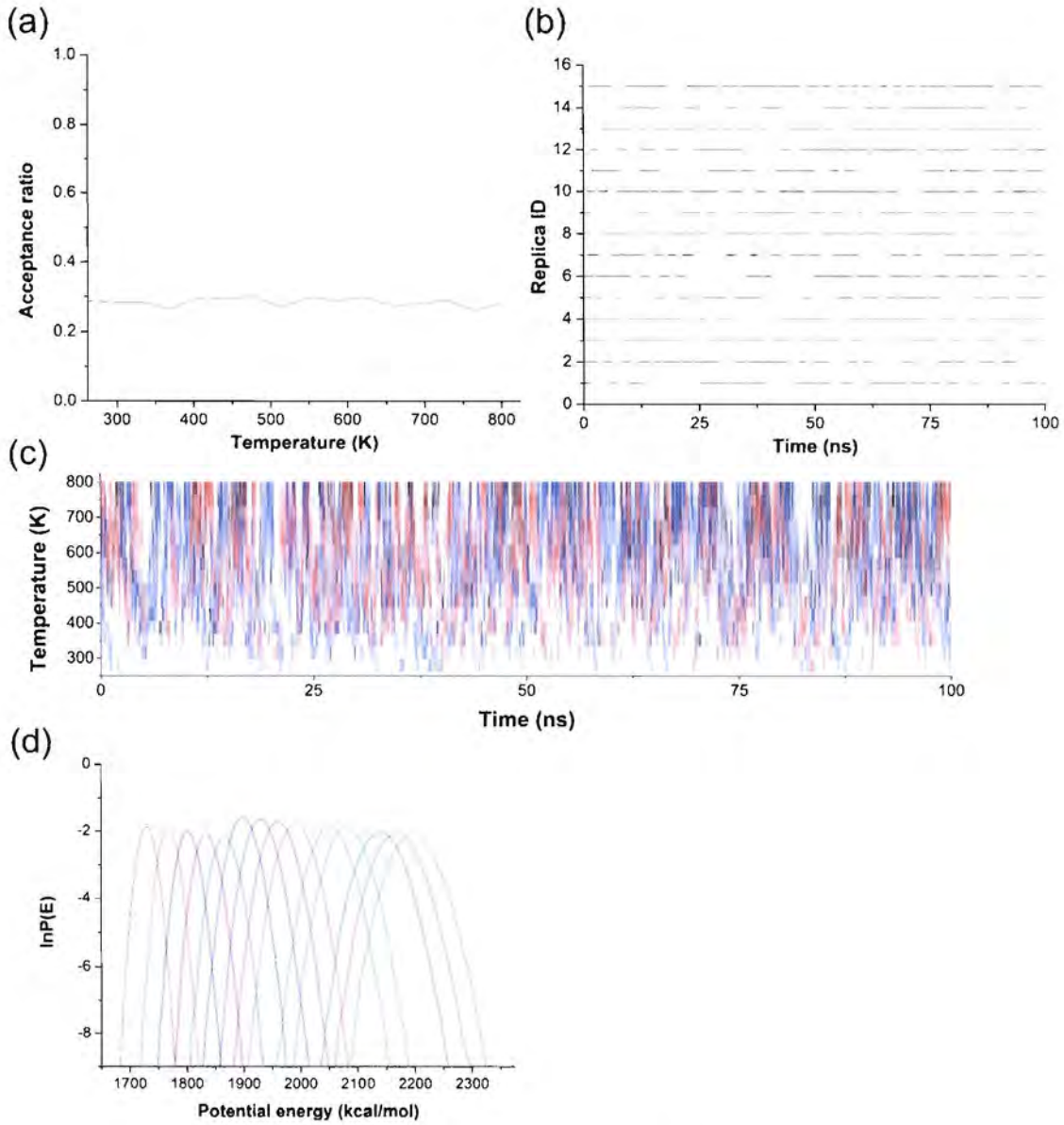

Fig 4. (a) The acceptance ratio of replica exchange of the adjacent pairs of the simulations of LFO_{15} in the GB_{HCT} model. **(b)** Replica exchange at 298 K. **(c)** Time series of temperature exchange of three arbitrary chosen replicas 2 (black), 8 (red) and 16 (blue). **(d)** The canonical probability of the total potential energy of the systems at 16 temperatures simulated in the GB_{HCT} model.

Sizes of LFOs

The sizes of LFOs were determined by measuring their radii of gyration. Fig. 5 shows that the trends of the radii of gyration of LFOs simulated in the GB_{HCT} model and those simulated in the GB_{OBC1} model were similar. The radii of gyration of LFOs tended to increase as their chain lengths increased from 5 to 15 residues. These results suggest the extension of the structures of LFOs as their chain lengths increase

.

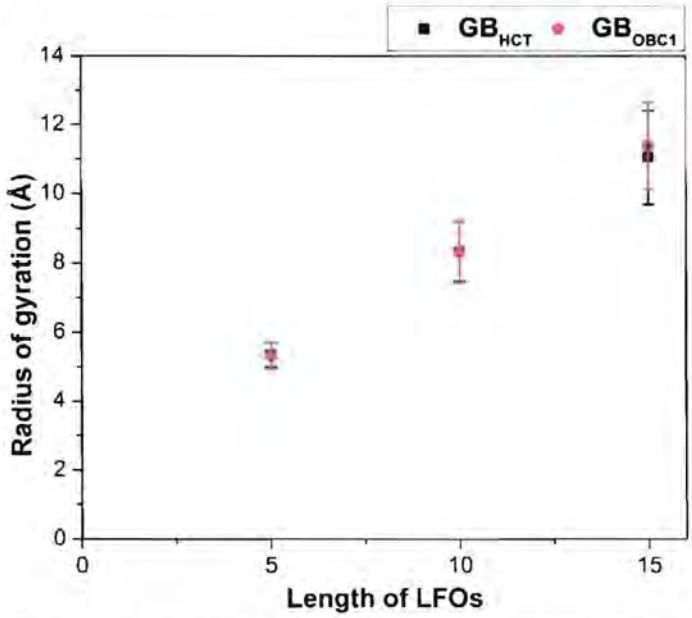

Fig 5. The average radii of gyration calculated from the heavy atoms of LFOs simulated in GB_{HCT} (square) and GB_{OBC1} (dot) models.

Conformations of LFO_{15}, LFO_{10} and LFO_5

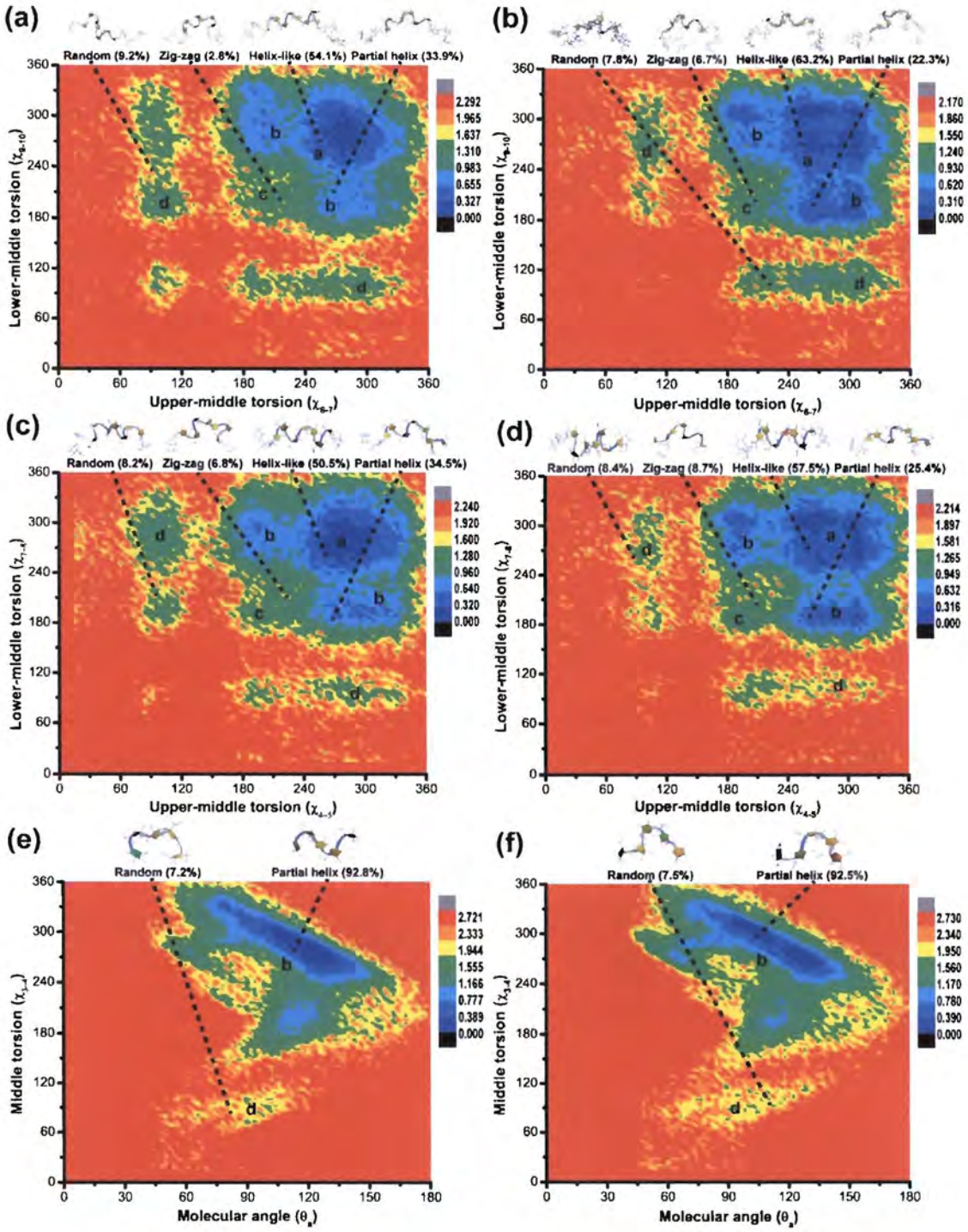

Fig 6. The relative free energy (kcal/mol) maps of LFO_{15} (a), LFO_{10} (c) and LFO_5 (e) simulated in the GB_{HCT} model as well as those of LFO_{15} (b), LFO_{10} (d) and LFO_5 (f) simulated in the GB_{OBC1} model. The groups a, b, c and d are helix-like, partial helix, zig-zag and random structures. Their major representative conformers and populations are also shown.

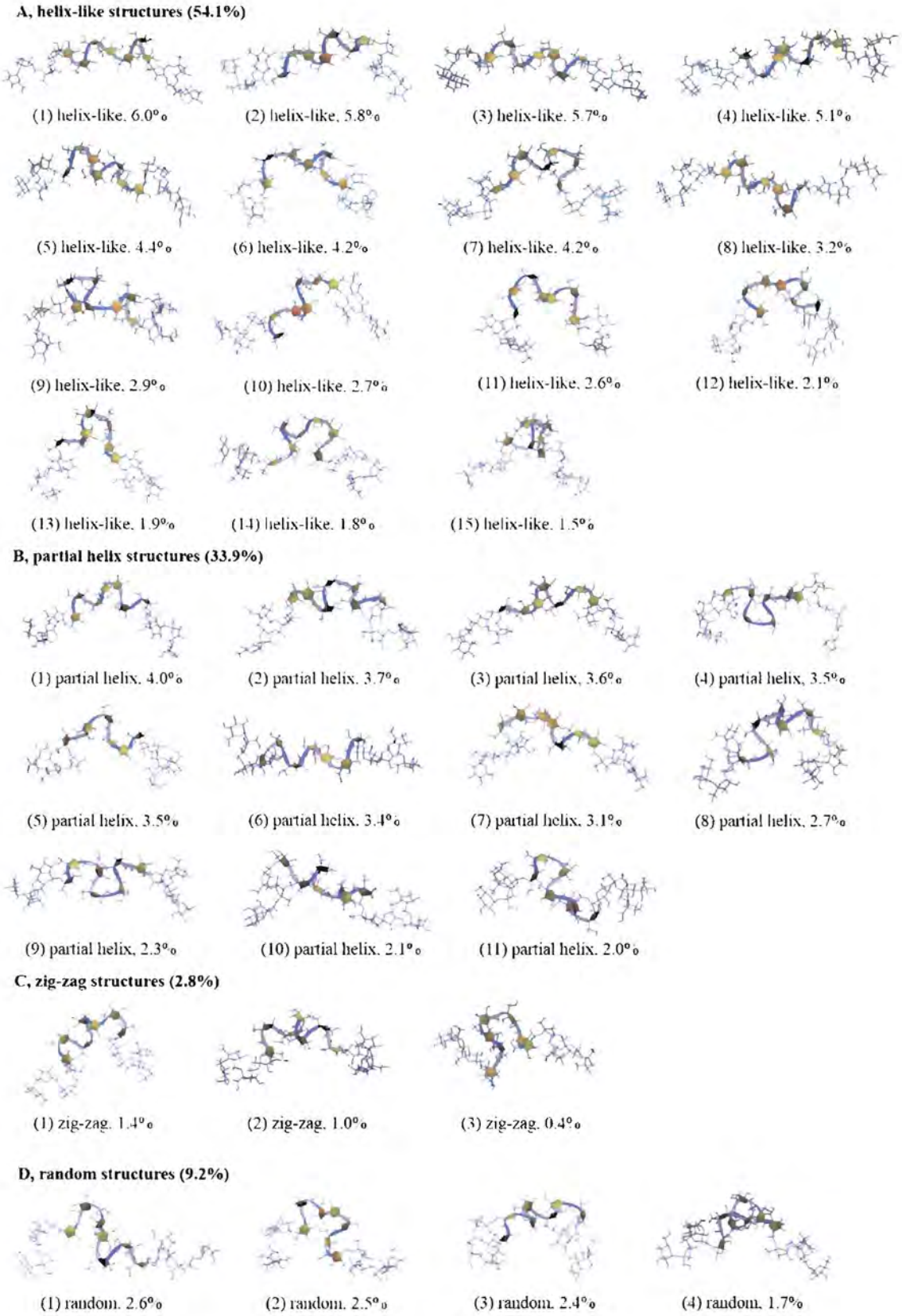

Fig 7. The "centroid" structure of each cluster of LFO_{15} simulated in the GB_{HCT} model. Their conformation types and populations are also shown.

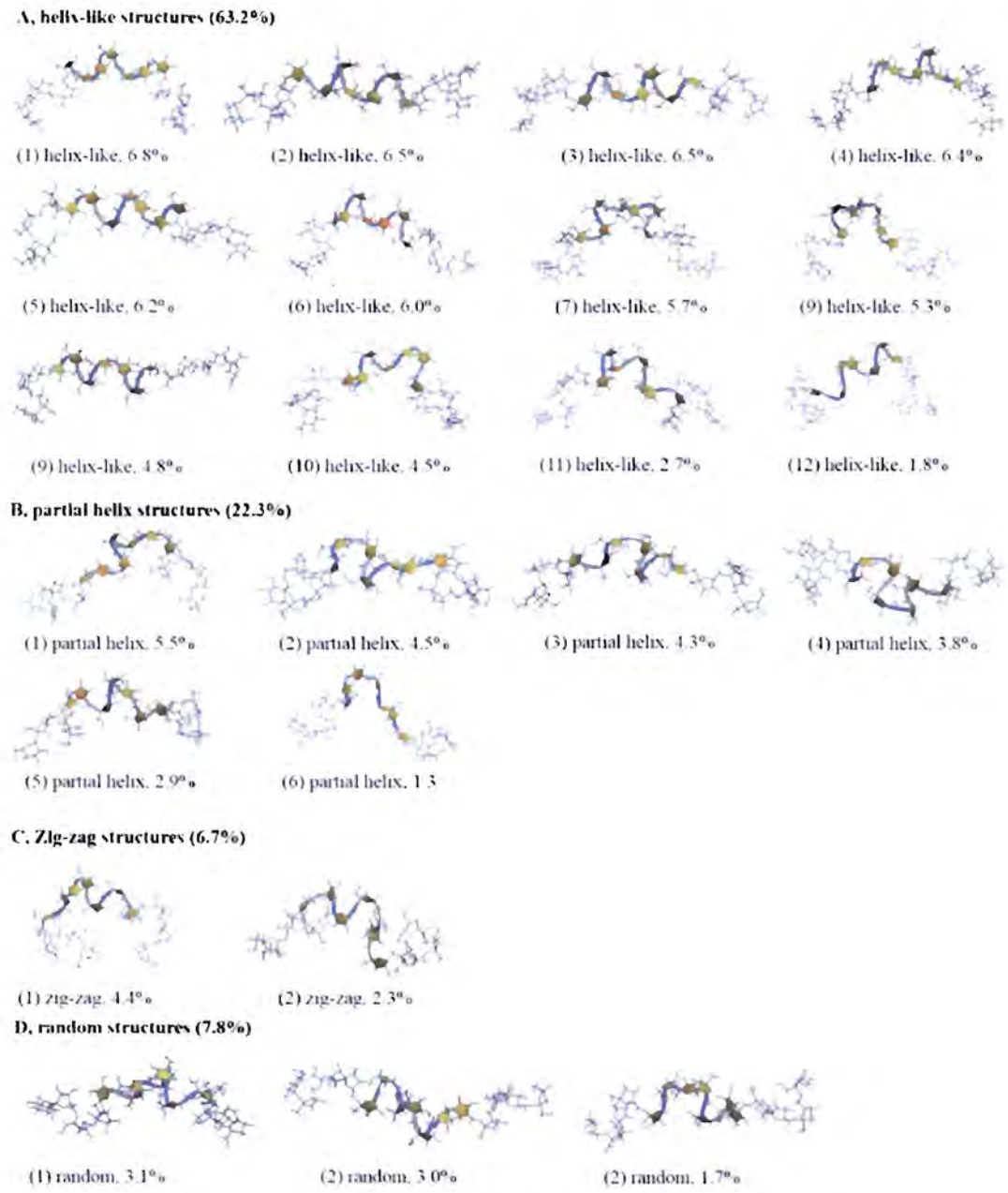

Fig 8. The "centroid" structure of each cluster of LFO_{15} simulated in the GB_{OBC1} model. Their conformation types and populations are also shown.

Fig. 6 shows the free-energy maps of LFO_{15}, LFO_{10} and LFO_5 as simulated in GB_{HTC} and GB_{OBC1} models as well as their major representative conformers and their population sizes from clustering analysis and centroid classification. For LFO_{15}, four major conformations such as helix-like (a), partial helix (b), zig-zag (c) and random (d) structures were observed after clustering analysis and centroid classification (Fig. 6(a, b) and Fig. 7 and 8), and they were characterized by their upper-middle and lower-middle torsions ($\chi_{6\text{-}7}$ and $\chi_{9\text{-}10}$). Helix-like structures were found with the highest population of 54.1% and 63.2% for those simulated in GB_{HCT} and GB_{OBC1} models,

respectively. Helix-like structures took up conformations of left-handed 3-fold helices and tended to have their upper-middle and lower-middle torsions in the similar range of around 240-315 degrees. The conformations with the second highest population were partial helix structures, and their population sizes were 33.9% and 22.3% for systems simulated in GB_{HCT} and GB_{OBC1} models, respectively. The other two conformations were zig-zag and random structures. Zig-zag structures were found with the population sizes of 2.8% and 6.7% for systems simulated in GB_{HCT} and GB_{OBC1} models, respectively. The population sizes of random structures simulated in GB_{HCT} and GB_{OBC1} models were 9.2% and 7.8%, respectively.

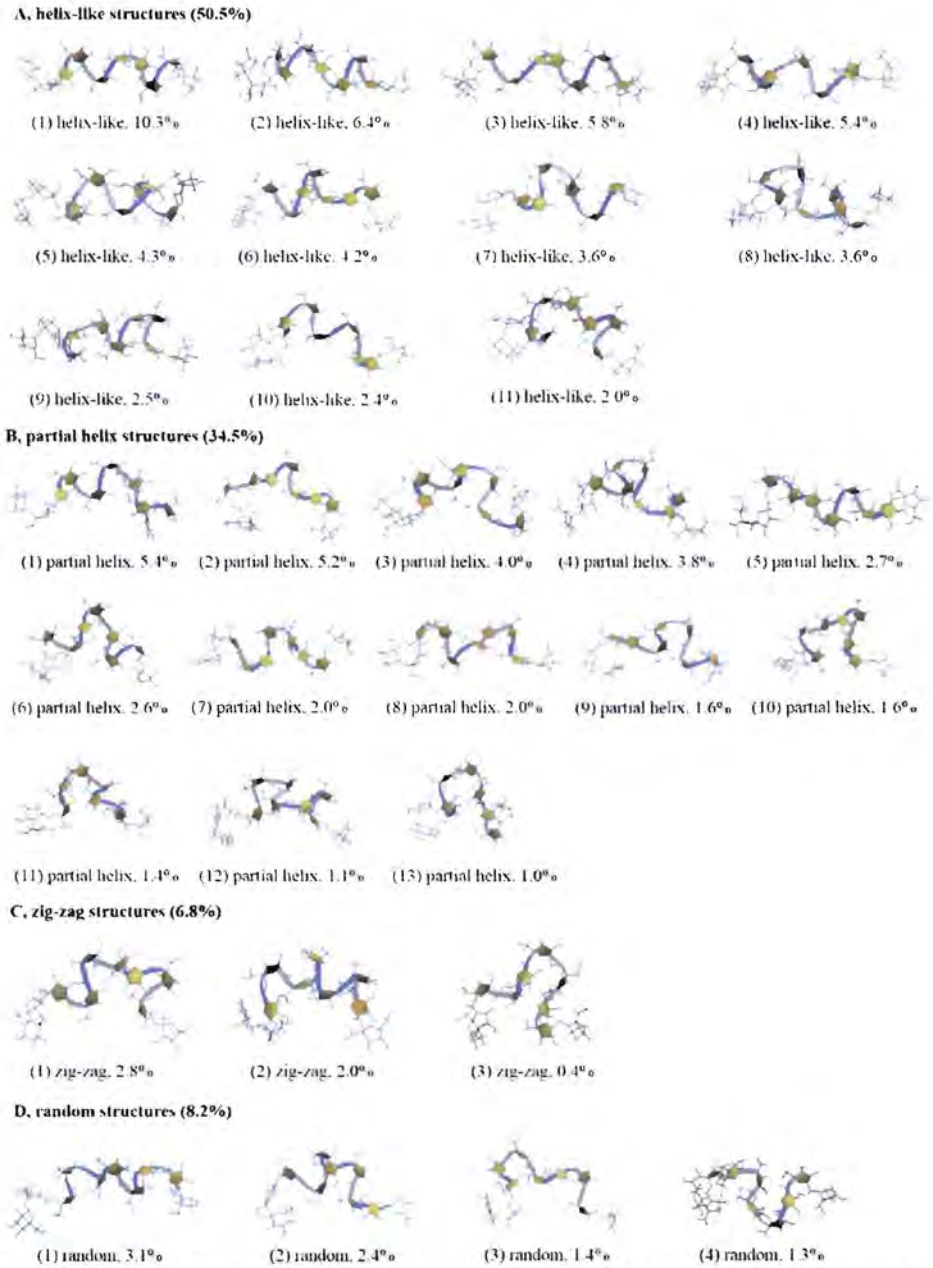

Fig 9. The "centroid" structure of each cluster of LFO_{10} simulated in the GB_{HCT} model. Their conformation types and populations are also shown.

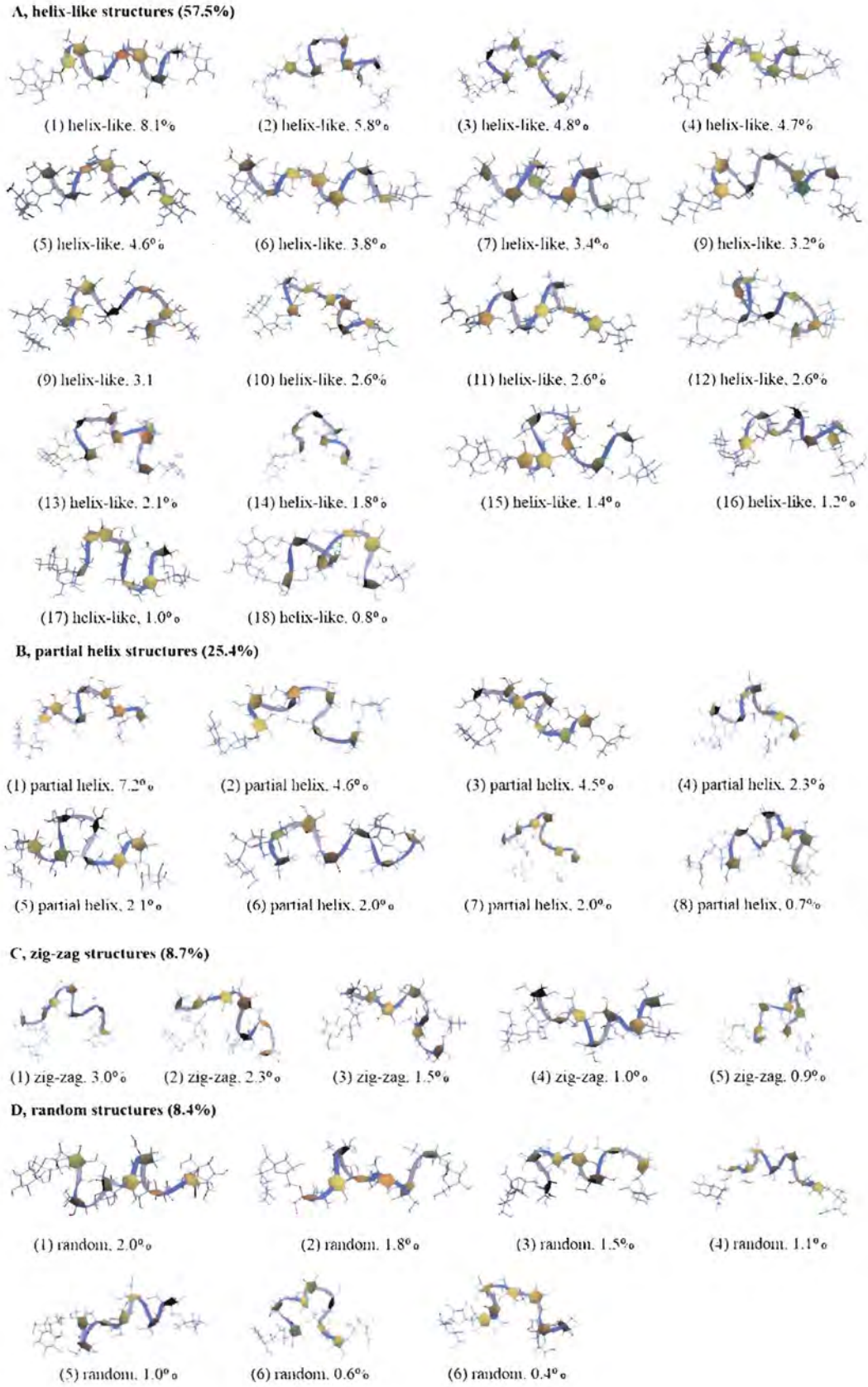

Fig 10. The "centroid" structure of each cluster of LFO_{10} simulated in the GB_{OBC1} model. Their conformation types and populations are also shown.

Similar to the conformations of LFO_{15}, four major conformations such as helix-like (a), partial helix (b), zig-zag (c) and random (d) structures were found for LFO_{10} after clustering analysis and centroid classification (Fig. 6(c, d) and Fig. 9 and 10). These conformations were characterized by their upper-middle and lower-middle torsions ($\chi_{4\text{-}5}$ and $\chi_{7\text{-}8}$). The conformation with the highest population sizes of 50.5% and 57.5% was helix-like structures for those simulated in GB_{HCT} and GB_{OBC1} models, respectively. Partial helix structures occurred with the second highest population sizes of 34.5% and 25.4% for those simulated in GB_{HCT} and GB_{OBC1} models, respectively. The population sizes of zig-zag structures were 6.8% and 8.7% and those of random structures were 8.2% and 8.4% for systems simulated in GB_{HCT} and GB_{OBC1} models, respectively.

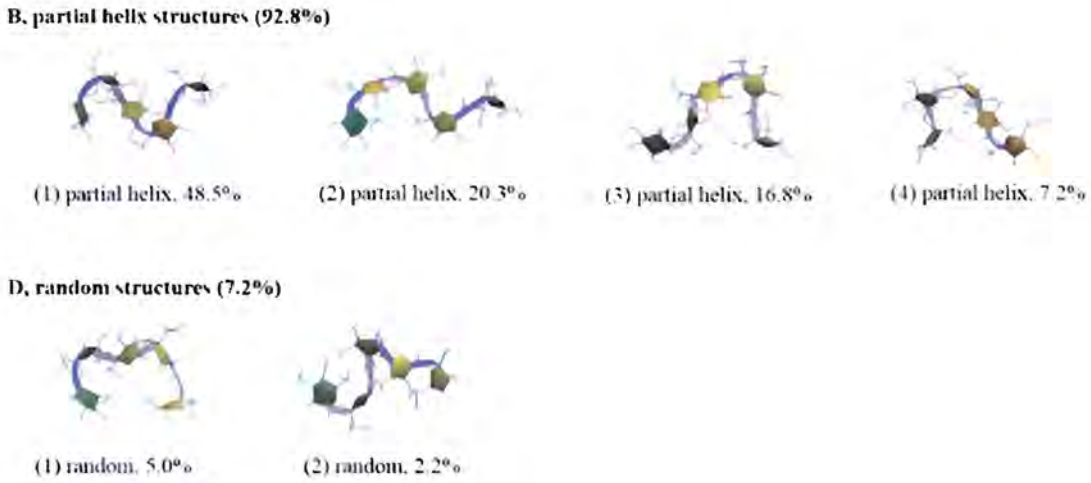

Fig 11. The "centroid" structure of each cluster of LFO_5 simulated in the GB_{HCT} model. Their conformation types and populations are also shown.

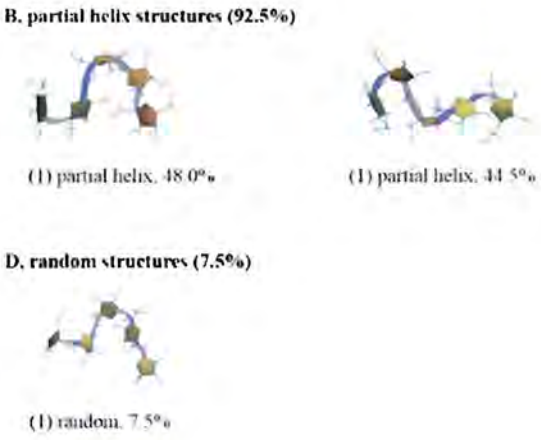

Fig 12. The "centroid" structure of each cluster of LFO_5 simulated in the GB_{OBC1} model. Their conformation types and populations are also shown.

For LFO_5, two major conformations such as partial helix (b) and random (d) structures were observed after clustering analysis and centroid classification, probably due to its shorter chain length as compared to those of LFO_{10} and LFO_{15} (Fig. 6(e, f) and Fig. 11 and 12). These conformations were characterized by their molecular angles (θ_a) and middle torsion ($\chi_{3\text{-}4}$). Partial helix structures were observed with the population sizes of 92.8% and 92.5% for those simulated in GB_{HCT} and GB_{OBC1} models, respectively. Random structures were also found with the population sizes of 7.2% and 7.5% for those simulated in GB_{HCT} and GB_{OBC1} models, respectively.

Table 4. The populations of major representative conformers of LFO_{15}, LFO_{10} and LFO_5 simulated in GB_{HCT} and GB_{OBC1} models as determined from clustering analysis and centroid classification.

Solvent model	Major representative conformer	Population (%)		
		LFO_{15}	LFO_{10}	LFO_5
GB_{HCT}	Helix-like structure	51.4	50.5	-
	Partial helix structure	33.9	34.5	92.8
	Zig-zag structure	2.8	6.8	-
	Random structure	9.2	8.2	7.2
GB_{OBC1}	Helix-like structure	63.2	57.5	-
	Partial helix structure	22.3	25.4	92.5
	Zig-zag structure	6.7	8.7	-
	Random structure	7.8	8.4	7.5

Table 4 shows the populations of major representative conformers of LFO_{15}, LFO_{10} and LFO_5 simulated in GB_{HCT} and GB_{OBC1} models as determined from clustering analysis and centroid classification. As the chain length increased, the population of the helix-like structures tended to increase. These results may suggest that LFOs have tendencies to form helices as their chain lengths are extended.

Hydrogen bonds important for the formation of helix-like structures

To elucidate the hydrogen bonds important for the formation of helix-like structures, the occurrence frequencies of hydrogen bonds in helix-like structures of LFO_{15} and LFO_{10} with the occurrence frequencies of at least 1% were analyzed. For the systems simulated in the GB_{HCT} model, the $O6_{(i)}$--$H3O_{(i+1)}$ hydrogen bonds (between residue i and i+1) were found with the highest frequency, and their glycosidic oxygens acted as important hydrogen bond acceptors that interacted with the hydroxyl groups of C3 atoms of the furanose rings and probably helped stabilize the helix-like structures (Table 5 and Fig. 13). The hydrogen bonds with the second and third highest occurrence frequencies for both LFO_{15} and LFO_{10} were the $O1_{(i)}$--$H3O_{(i)}$ and $O5_{(i)}$--$H1O_{(i)}$ hydrogen bonds, which were the hydrogen bonds within the same residue (Table 2 and Fig. 4). The trends of the occurrence frequencies of the hydrogen bonds of LFO_{15} and LFO_{10} in the GB_{OBC1} model were also similar to those in the GB_{HCT} model (Table 2). These three hydrogen bonds ($O6_{(i)}$--$H3O_{(i+1)}$, $O1_{(i)}$--$H3O_{(i)}$ and $O5_{(i)}$--$H1O_{(i)}$ hydrogen bonds), especially the $O6_{(i)}$--$H3O_{(i+1)}$ hydrogen bond that was found with the highest frequency, are probably important for the formation of helix-like structures of LFO_{15} and LFO_{10} as their occurrence frequencies are higher than other hydrogen bonds.

Table 5. Occurrence frequencies of hydrogen bonds found in helix-liked structures of LFO_{15} and LFO_{10}.

Solvent model	Residue that form a hydrogen bond	Type	Occurrence frequency[a] (%)	
			LFO_{15}	LFO_{10}
GB_{HCT}	i, i	$O1_{(i)}$-$H3O_{(i)}$	15.4	15.3
		$O5_{(i)}$-$H1O_{(i)}$	11.5	12.5
	i, (i + 1)	$O6_{(i)}$-$H3O_{(i+1)}$	65.0	60.2
GB_{OBC1}	i, i	$O1_{(i)}$-$H3O_{(i)}$	10.0	10.0
		$O5_{(i)}$-$H1O_{(i)}$	8.3	7.8
	i, (i + 1)	$O6_{(i)}$-$H3O_{(i+1)}$	37.5	34.8

[a]Only hydrogen bonds with the occurrence frequency of at least 7 % are shown

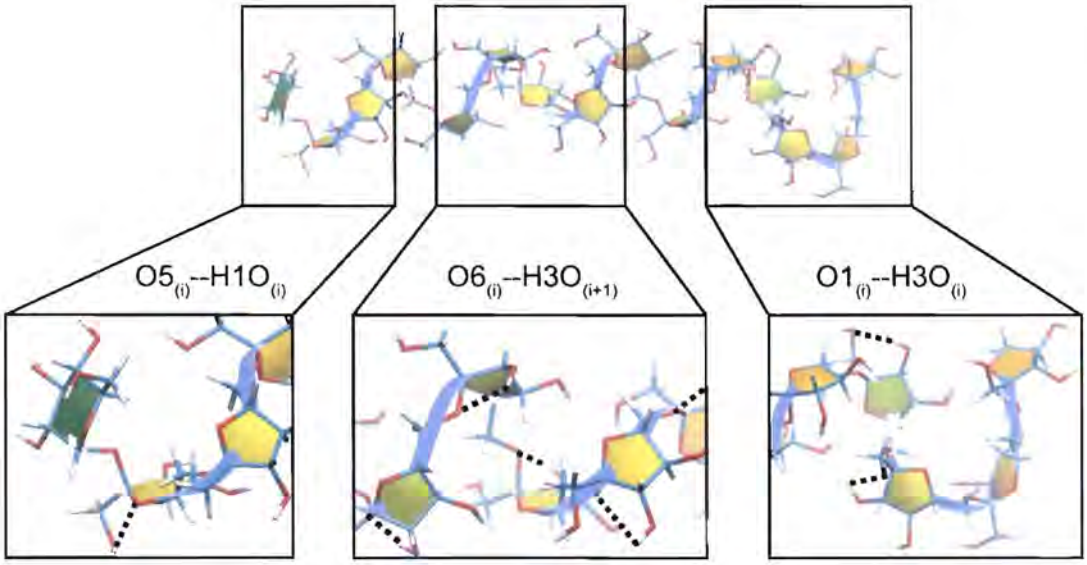

Fig 13. Hydrogen bonds important for the formation of helix-like structures (LFO_{15} simulated in the GB_{HCT} model is shown as an example). Middle; the $O6_{(i)}$--$H3O_{(i+1)}$ hydrogen bond (occurrence frequency = 65.0%). Right; the $O1_{(i)}$--$H3O_{(i)}$ hydrogen bond. (occurrence frequency = 15.4%). Left; the $O5_{(i)}$--$H1O_{(i)}$ hydrogen bond (occurrence frequency = 11.5%). Hydrogen bonds are represented as dash lines. The LFO chain and fructosyl units are represented as ribbon and filled yellow color representations, respectively.

Conformational flexibilities

To investigate the conformational flexibilities of LFO_{15}, LFO_{10} and LFO_5, the occurrence frequencies of ω, ψ and ϕ of all glycosidic bonds were measured. For the systems simulated in the GB_{HCT} model, ψ and ϕ of all glycosidc linkages of all LFOs exhibited single major peaks around 173° and -63°, respectively (Fig. 14). However, ω was more flexible than ψ and ϕ as it exhibited one major peak and two minor peaks (Fig. 14). The results from the systems simulated in the GB_{OBC1} model were similar (Fig. 15); ω exhibited more peaks and was more flexible than ψ and ϕ. These results suggest that the flexibility of ω may be responsible for the conformational diversity of LFOs since this dihedral angle has more possibilities in rotating and changing the conformations of LFOs.

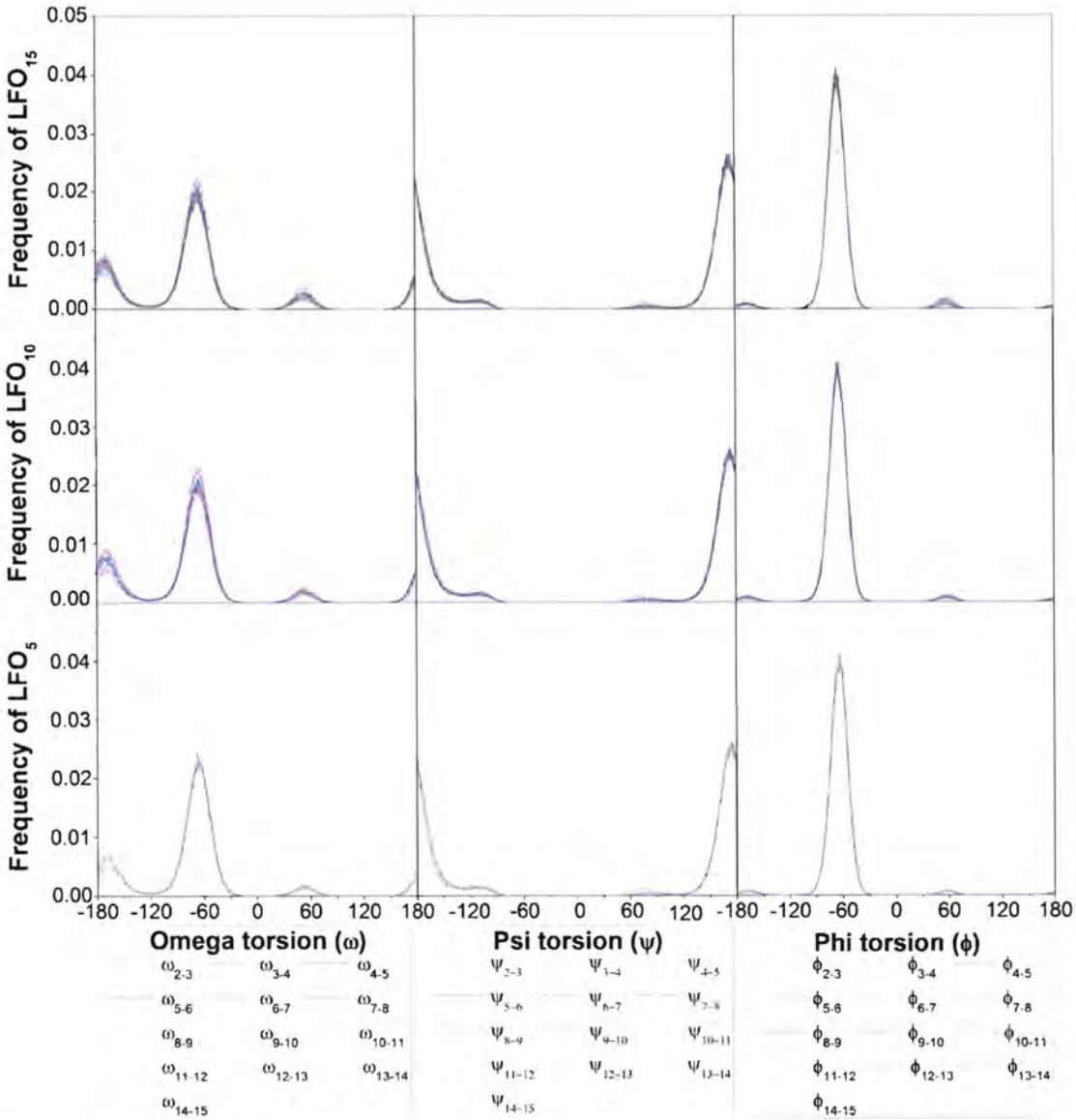

Fig 14. The frequencies of the three dihedral angles of all glycosidic linkage of LFO_{15}, LFO_{10} and LFO_5 in the GB_{HCT} model. Each dihedral angle is shown in different color.

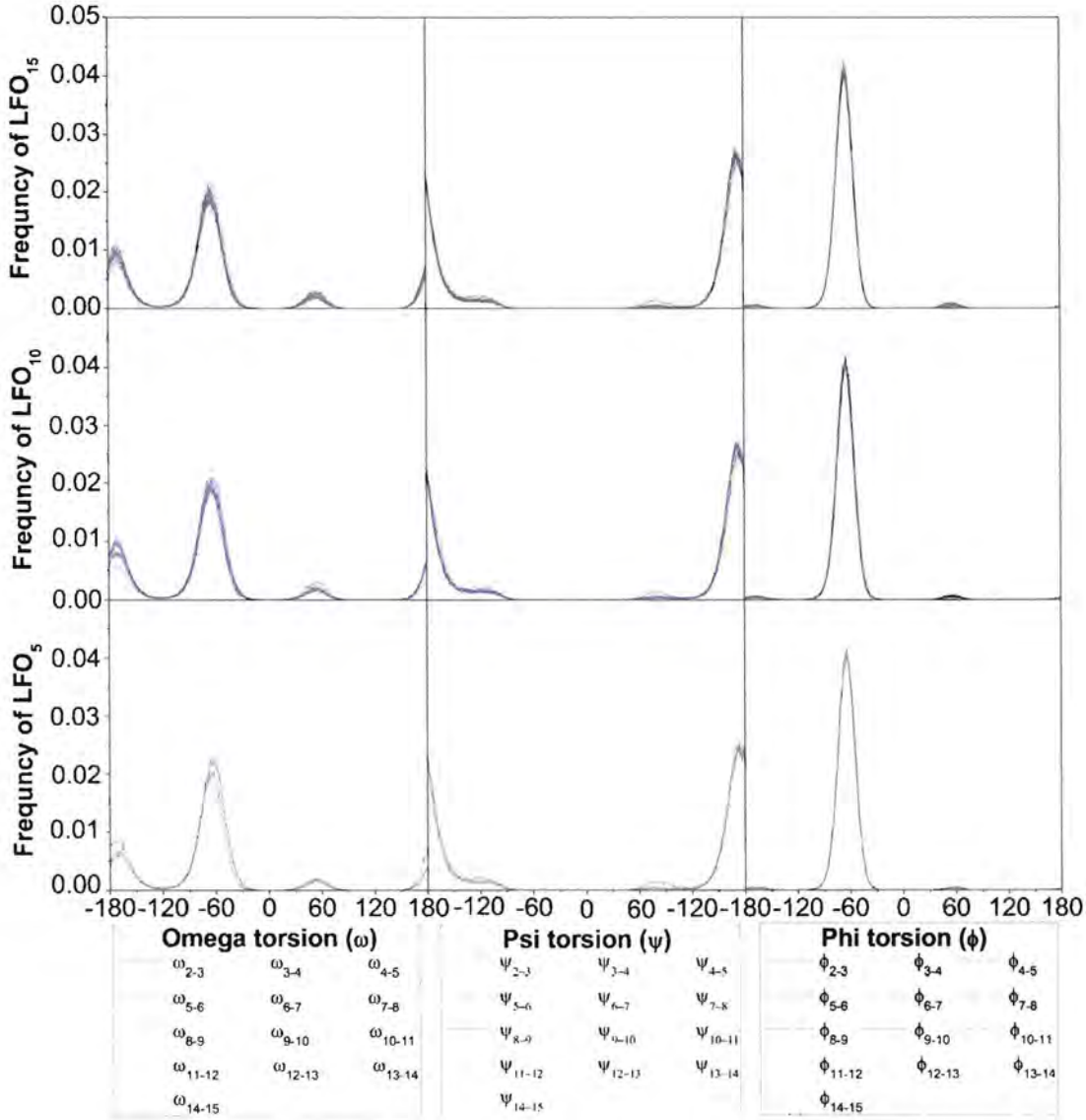

Fig 15. The frequencies of the three dihedral angles of all glycosidic linkage of LFO_{15}, LFO_{10} and LFO_5 in the GB_{OBC1} model. Each dihedral angle is shown in different color.

Conclusions

To elucidate the structural and molecular properties of LFOs as well as the relationship between these properties and their chain lengths, REMD were performed on systems of LFO_5, LFO_{10} and LFO_{15} in GB_{HCT} and GB_{OBC1} solvent models. We found that as the chain length increased, the radii of gyration tended to increase, suggesting the extension of the conformations as the chain length increases. After clustering analysis and centroid classifications, four major representative conformations (helix-like, partial helix, zig-zag and random structures) were found for LFO_{15} and LFO_{10}, while two conformations (partial helix and random structures) were identified for LFO_5. The free energy map shows that the four conformations of LFO_{15} and LFO_{10} were characterized by their upper-middle and lower-middle torsions, whereas the two conformations of LFO_5 were characterized by their molecular angles and middle torsions. As the chain length increased from 5 to 15 residues, the conformation populations of the helix-like structures tended to increase, suggesting the possible tendency of LFOs to form helices as their chain lengths are extended. Moreover, the $O6_{(i)}$--$H3O_{(i+1)}$ hydrogen bond was found with the highest frequency, suggesting its importance in helix formation of LFO_{15} and LFO_{10}. Furthermore, ω was found to be more flexible than ψ and ϕ and probably responsible for the conformational diversity of LFOs. This study gives an important insight into the structural and molecular properties of LFOs; they tend to form helical structures as the chain length increases from 5 to 15 residues. Our findings may be useful in the selection of LFOs with appropriate chain lengths and structural properties for pharmaceutical and biological applications.

Suggestions for future work

To increase the knowledge on the structural and molecular properties of LFOs, REMD of LFOs with the chain length of more than 15 residues can be performed. Moreover, since the structural and molecular properties of LFOs also depend on the branching degrees, REMD of LFOs with various branching degrees should also be investigated.

Output from research project funded by TRF

1. Publication in international journal (BMC Bioinformatics, IF 2015 = 2.435, Q1 in Mathematical & Computational Biology)

   -Kanjanatanin, P, Pichyangkura, R, **Chunsrivirot, S.** (2016). Replica exchange molecular dynamics simulations reveal the structural and molecular properties of levan-type fructo-oligosaccharides of various chain lengths. *BMC Bioinformatics*, 17, 306.

2. Conference presentations

   - Dr. Surasak Chunsrivirot was invited to give an oral presentation entitled "Elucidation of the structural and molecular properties of levan-type fructo-oligosaccharides with the chain lengths of 5, 10 and 15 residues" at the 2nd CU-NAIST Symposium 2015 at Chulalongkorn University, Bangkok on Dec 16th 2015.

   - Mr. Pongsakorn Kanjanatanin (PhD student) gave an oral presentation entitled "the structural and molecular properties of levan-type fructo-oligosaccharides with chain lengths of 5, 10 and 15 residues as revealed by replica-exchange molecular dynamics simulations" at the Pure and Applied Chemistry International Conference at BITEC, Bangkok on Feb 10th, 2016.

   - Dr. Surasak Chunsrivirot gave an oral presentation entitled "Replica exchange molecular dynamics simulations reveal the structural and molecular properties of levan-type fructo-oligosaccharides of various chain lengths" at the 5th International conference on Biotechnology and Bioengineering at Mandarin hotel, Bangkok on Dec 10th, 2016.

References

1. Steinmetz, M., Le Coq, D., Aymerich, S., Gonzy-Tréboul, G., and Gay, P. (1985) The DNA sequence of the gene for the secreted *Bacillus subtilis* enzyme levansucrase and its genetic control sites, *Molecular and General Genetics 200*, 220-228.
2. Goldman, D., Lavid, N., Schwartz, A., Shoham, G., Danino, D., and Shoham, Y. (2008) Two Active Forms of *Zymomonas mobilis* Levansucrase AN ORDERED MICROFIBRIL STRUCTURE OF THE ENZYME PROMOTES LEVAN POLYMERIZATION, *Journal of Biological Chemistry 283*, 32209-32217.
3. Martínez-Fleites, C., Ortiz-Lombardía, M., Hernandez, L., Pons, T., Tarbouriech, N., Taylor, E., Arrieta, J., and Davies, G. x. a. j. (2005) Crystal structure of levansucrase from the Gram-negative bacterium *Gluconacetobacter diazotrophicus*, *Biochemical Journal 390*, 19-27.
4. Hettwer, U., Jaeckel, F. R., Boch, J., Meyer, M., Rudolph, K., and Ullrich, M. S. (1998) Cloning, Nucleotide Sequence, and Expression in *Escherichia coli* of Levansucrase Genes from the Plant Pathogens *Pseudomonas syringae pv. glycinea* and *P. syringaepv. phaseolicola*, *Applied and environmental microbiology 64*, 3180-3187.
5. Song, K. B., Seo, J. W., Kim, M. G., and Rhee, S. K. (1998) Levansucrase of *Rahnella aquatilis* ATCC33071: gene cloning, expression, and levan formation, *Annals of the New York Academy of Sciences 864*, 506-511.
6. Kang, H. K., Seo, M. Y., Seo, E. S., Kim, D., Chung, S. Y., Kimura, A., Day, D. F., and Robyt, J. F. (2005) Cloning and expression of levansucrase from *Leuconostoc mesenteroides* B-512 FMC in *Escherichia coli*, *Biochimica et Biophysica Acta (BBA)-Gene Structure and Expression 1727*, 5-15.
7. Arvidson, S. A., Rinehart, B. T., and Gadala-Maria, F. (2006) Concentration regimes of solutions of levan polysaccharide from *Bacillus* sp., *Carbohydrate polymers 65*, 144-149.
8. Han, Y. W. (1990) Microbial levan, *Advances in Applied Microbiology 35*, 171-194.
9. Yamamoto, Y., Takahashi, Y., Kawano, M., Iizuka, M., Matsumoto, T., Saeki, S., and Yamaguchi, H. (1999) In vitro digestibility and fermentability of levan and its hypocholesterolemic effects in rats, *The Journal of Nutritional Biochemistry 10*, 13-18.

10. Marx, S. P., Winkler, S., and Hartmeier, W. (2000) Metabolization of β-(2, 6)-linked fructose-oligosaccharides by different bifidobacteria, *Federation of European Microbiological Societies Microbiology Letters 182*, 163-169.

11. Marchessault, R. H., Ravenelle, F., and Zhu, X. X. (2006) *Polysaccharides for drug delivery and pharmaceutical applications*, Vol. 934, An American Chemical Society Publication.

12. Esawy, M. A., Ahmed, E. F., Helmy, W. A., Mansour, N. M., El-Senousy, W. M., and El-Safty, M. M. (2011) Production of levansucrase from novel honey *Bacillus subtilis* isolates capable of producing antiviral levans, *Carbohydrate polymers 86*, 823-830.

13. Yoo, S.-H., Yoon, E. J., Cha, J., and Lee, H. G. (2004) Antitumor activity of levan polysaccharides from selected microorganisms, *International Journal of Biological Macromolecules 34*, 37-41.

14. Yoon, E. J., Yoo, S.-H., Cha, J., and Gyu Lee, H. (2004) Effect of levan's branching structure on antitumor activity, *International Journal of Biological Macromolecules 34*, 191-194.

15. Nakapong, S. (2011) Biochemical and structural characterization of levansucrase from *Bacillus licheniformis* RN-01., In *Biochemistry*, Chulalongkorn University, Bangkok.

16. Kang, S. A., Jang, K.-H., Seo, J.-W., Kim, K. H., Kim, Y. H., Rairakhwada, D., Seo, M. Y., Lee, J. O., Do, S., and Ha, C. H. K. (2009) Levan: applications and perspectives, *Microbial production of biopolymers and polymer precursors. Caister Academic Press, Norwich*, 145-161.

17. Franca, E. F., Freitas, L. C., and Lins, R. D. (2011) Chitosan molecular structure as a function of N-acetylation, *Biopolymers 95*, 448-460.

18. Franca, E. F., Lins, R. D., Freitas, L. C., and Straatsma, T. (2008) Characterization of chitin and chitosan molecular structure in aqueous solution, *Journal of Chemical Theory and Computation 4*, 2141-2149.

19. Sorlier, P., Denuzière, A., Viton, C., and Domard, A. (2001) Relation between the degree of acetylation and the electrostatic properties of chitin and chitosan, *Biomacromolecules 2*, 765-772.

20. Kadirvelraj, R., Foley, B. L., Dyekjær, J. D., and Woods, R. J. (2008) Involvement of water in carbohydrate– protein binding: Concanavalin A revisited, *Journal of the American Chemical Society 130*, 16933-16942.

21. Sattelle, B. M., and Almond, A. (2014) Shaping up for structural glycomics: a predictive protocol for oligosaccharide conformational analysis applied to N-linked glycans, *Carbohydrate research 383*, 34-42.

22. Pendrill, R., Sawen, E., and Widmalm, G. (2013) Conformation and Dynamics at a Flexible Glycosidic Linkage Revealed by NMR Spectroscopy and Molecular Dynamics Simulations: Analysis of beta-L-Fucp-(1 -> 6)-alpha-D-Glcp-OMe in Water Solution, *J. Phys. Chem. B 117*, 14709-14722.

23. Wu, E. L., Engstrom, O., Jo, S., Stuhlsatz, D., Yeom, M. S., Klauda, J. B., Widmalm, G., and Im, W. (2013) Molecular Dynamics and NMR Spectroscopy Studies of E. coli Lipopolysaccharide Structure and Dynamics, *Biophys. J. 105*, 1444-1455.

24. Earl, D. J., and Deem, M. W. (2005) Parallel tempering: Theory, applications, and new perspectives, *Physical Chemistry Chemical Physics 7*, 3910-3916.

25. Shen, T., Langan, P., French, A. D., Johnson, G. P., and Gnanakaran, S. (2009) Conformational flexibility of soluble cellulose oligomers: chain length and temperature dependence, *Journal of the American Chemical Society 131*, 14786-14794.

26. Nishima, W., Miyashita, N., Yamaguchi, Y., Sugita, Y., and Re, S. (2012) Effect of Bisecting GlcNAc and Core Fucosylation on Conformational Properties of Biantennary Complex-Type N-Glycans in Solution, *J. Phys. Chem. B 116*, 8504-8512.

27. Re, S., Miyashita, N., Yamaguchi, Y., and Sugita, Y. (2011) Structural Diversity and Changes in Conformational Equilibria of Biantennary Complex-Type N-Glycans in Water Revealed by Replica-Exchange Molecular Dynamics Simulation, *Biophys. J. 101*, L44-L46.

28. Ferrara, P., Apostolakis, J., and Caflisch, A. (2002) Evaluation of a fast implicit solvent model for molecular dynamics simulations, *Proteins: Structure, Function, and Bioinformatics 46*, 24-33.

29. Rungnim, C., Rungrotmongkol, T., Hannongbua, S., and Okumura, H. (2013) Replica exchange molecular dynamics simulation of chitosan for drug delivery system based on carbon nanotube, *Journal of molecular graphics and modelling 39*, 183-192.

30. Case, D., Babin, V., Berryman, J., Betz, R., Cai, Q., Cerutti, D., Cheatham III, T., Darden, T., Duke, R., and Gohlke, H. AMBER 14, 2014, *University of California, San Francisco Search PubMed*.

31. Kirschner, K. N., Yongye, A. B., Tschampel, S. M., González-Outeiriño, J., Daniels, C. R., Foley, B. L., and Woods, R. J. (2008) GLYCAM06: a generalizable biomolecular force field. Carbohydrates, *J. Comput. Chem. 29*, 622-655.

32. Hawkins, G. D., Cramer, C. J., and Truhlar, D. G. (1996) Parametrized models of aqueous free energies of solvation based on pairwise descreening of solute atomic charges from a dielectric medium, *J. Phys. Chem. 100*, 19824-19839.

33. Onufriev, A., Bashford, D., and Case, D. A. (2000) Modification of the generalized Born model suitable for macromolecules, *J. Phys. Chem. B. 104*, 3712-3720.

34. Cerutti, D. S., Duke, R., Freddolino, P. L., Fan, H., and Lybrand, T. P. (2008) A vulnerability in popular molecular dynamics packages concerning Langevin and Andersen dynamics, *J. Chem. Theory Comput. 4*, 1669-1680.

35. Ryckaert, J.-P., Ciccotti, G., and Berendsen, H. J. (1977) Numerical integration of the cartesian equations of motion of a system with constraints: molecular dynamics of n-alkanes, *J. Comput. Phys. 23*, 327-341.

36. Feig, M., Karanicolas, J., and Brooks, C. L. (2004) MMTSB Tool Set: enhanced sampling and multiscale modeling methods for applications in structural biology, *J. Mol. Graph. Model. 22*, 377-395.

Kanjanatanin *et al. BMC Bioinformatics* (2016) 17:306
DOI 10.1186/s12859-016-1182-7

BMC Bioinformatics

RESEARCH ARTICLE Open Access

Replica exchange molecular dynamics simulations reveal the structural and molecular properties of levan-type fructo-oligosaccharides of various chain lengths

Pongsakorn Kanjanatanin[1,2], Rath Pichyangkura[1] and Surasak Chunsrivirot[1,2*]

Abstract

Background: Levan and levan-type fructo-oligosaccharides (LFOs) have various potential applications in pharmaceutical and food industries due to their beneficial properties such as their low intrinsic viscosity and high water solubility. Previous studies showed that they exhibited prebiotic effects, anti-inflammatory and anti-tumor activities against Sarcoma-180 tumor cells of human. Despite their various potential applications, the structural and molecular properties of LFOs of various chain lengths are not well understood.

Results: We employed the replica-exchange molecular dynamics simulations method (REMD) in AMBER14 to elucidate structural and molecular properties of LFOs with chain lengths of 5 (LFO_5), 10 (LFO_{10}) and 15 (LFO_{15}) residues in two models of generalized Born implicit solvent (GB_{HCT} and GB_{OBC1}). For LFO_{10} and LFO_{15}, four distinct conformations (helix-like, partial helix, zig-zag and random structures) were characterized by their upper-middle and lower-middle torsions. For LFO_5, two distinct conformations (partial helix and random structures) were characterized by their middle torsion and molecular angle of residues 1, 3 and 5. To determine hydrogen bonds important for the formation of helix-like structures of LFO_{10} and LFO_{15}, occurrence frequencies of hydrogen bonds were analyzed, and the $O6_{(i)}$–$H3O_{(i+1)}$ hydrogen bond was found with the highest frequency, suggesting its importance in helix formation. Among three dihedral angles between two fructosyl units [ϕ (O5′-C2′-O6-C6), ψ (C2′-O6-C6-C5) and ω (O6-C6-C5-C4)], dihedral angle distributions showed that ω was the most flexible dihedral angle and probably responsible for conformational differences of LFOs.

Conclusions: Our study provides important insights into the structural and molecular properties of LFOs, which tend to form helical structures as the chain length increases from 5 to 15 residues. This information could be beneficial for the selection of LFOs with appropriate lengths and properties for pharmaceutical and biological applications.

Keywords: Levan, Helix, Replica exchange molecular dynamics simulation, Oligosaccharide, Generalized Born implicit solvent

Abbreviations: GB, Generalized Born implicit solvent; LFOs, Levan-type fructo-oligosaccharides; REMD, Replica-exchange molecular dynamics simulations.

* Correspondence: surasak.ch@chula.ac.th
[1]Department of Biochemistry, Faculty of Science, Chulalongkorn University, 254 Phaya Thai road, Pathumwan, Bangkok 10330, Thailand
[2]Structural and Computational Biology Research Group, Department of Biochemistry, Faculty of Science, Chulalongkorn University, 254 Phaya Thai road, Pathumwan, Bangkok 10330, Thailand

Background

Levan-type fructo-oligosaccharides (LFOs) are short chain fructans that contain D-fructofuranosyl residues and are predominantly linked by β-(2, 6) linkages in a main chain with some β-(2, 1) linked branching points (Fig. 1a). Produced by levansucrase, levan and LFOs are found in various microorganisms such as *Bacillus subtilis* [1], *Zymomonas mobilis* [2], and *Leuconostoc mesenteroides* [3], and play important roles as sources for energy utilization and biofilm formation [4, 5]. The properties of levan and LFOs depend on their chain lengths and branching degrees [6], and they have various desirable properties such as their unusually low intrinsic viscosity [7] and high water solubility [8]. These properties are very beneficial for various industrial applications, especially in food and pharmaceutical industries. For example, levan and LFOs showed prebiotic effects, stimulating the growth of beneficial intestinal bacteria, and also could potentially act as cholesterol lowering agents (MW 2000 kDa) [9, 10]. Furthermore, they could also be served as carbon sources for probiotics such as four strains of *Bifidobacterium sp.* that produce short chain fatty acids, lactate and acetate (MW < 3600 Da) [11]. Moreover, they exhibited anti-inflammatory and anti-tumor activities against Sarcoma-180 tumor cells of human (MW 380–710 kDa) [12, 13]. Despite their various potential applications, the knowledge on the structural and molecular properties of levan and LFOs of various chain lengths is still limited.

Replica exchange molecular dynamics (REMD) method provides an extensive conformational sampling at various temperatures by allowing each replica to exchange their configurations through parallel tempering [14]. Raising the temperature can increase the probability of the system to overcome the energy barrier, consequently enhancing the probability of attaining the global minimum and allowing the sampling of large volumes of phase space. Therefore, the incorporation of higher temperature systems allow the lower temperature systems to access a representative set of the low free energy minima that are accessible by the higher temperature systems [15]. This technique has been used to investigate the properties of oligosaccharides in solution. For example, Re *et al.* employed REMD to elucidate the structural diversity and the changes in conformational equilibria of biantennary

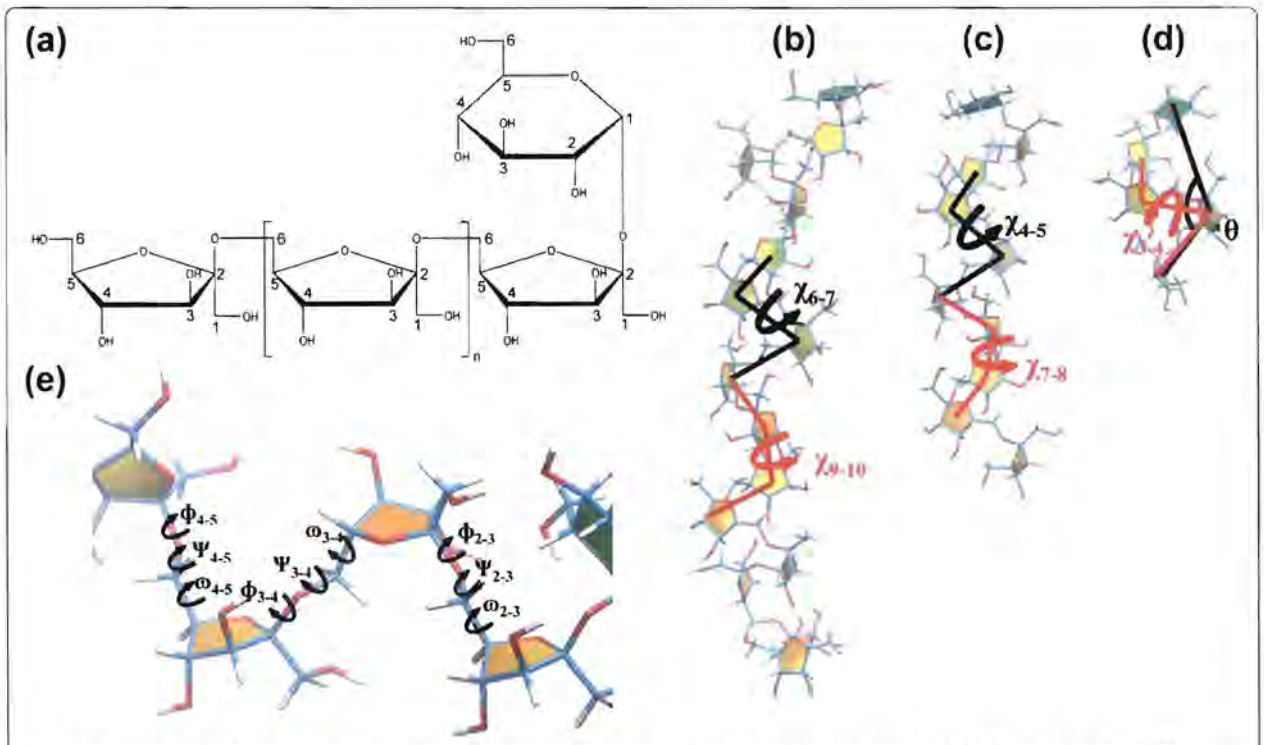

Fig. 1 An example of LFO structure and the parameters used in the characterization of the conformations of LFOs. (**a**) An example of LFO structure with no branch. (**b**) The parameters used in the characterization of the conformations of LFOs: the upper-middle (χ_{6-7}) and lower-middle (χ_{9-10}) torsions for LFO_{15}, (**c**) the upper-middle (χ_{4-5}) and lower-middle (χ_{7-8}) torsions for LFO_{10}, (**d**) the molecular angles (θ_a) and middle torsions (χ_{3-4}) for LFO_5. (**e**) Examples of three dihedral angles between four fructosyl residues of LFO_5, ω (C4-C5-C6-O6), ψ (C5-C6-O6-C2') and ϕ (C6-O6-C2'-O5'). The carbon, oxygen and hydrogen atoms were colored in green, red and white, respectively. The six-membered ring of the glucosyl residue and the five-membered rings of fructosyl residue are shown in green and yellow, respectively

complex-type N-glycans [16]. Moreover, Nishima *et al.* used this technique to investigate the effects of bisecting GlcNAc and core fucosylation on conformational properties of biantennary complex-type N-glycans [17]. Recently, Jo *et al.* employed this technique to examine the conformational freedom of the N-glycan core pentasaccharide moiety in solution and found that the conformational variability of the pentasaccharide in solution was more restricted than the *N*-glycan on the protein surface [18]. This method was also employed to investigate conformational flexibility of cellulose oligomers as well as their chain length and temperature dependence [19]. However, to our knowledge, REMD method has not been used in the elucidation of the properties of LFOs of various chain lengths.

In this study, we performed REMD on the models of LFOs with the chain lengths of 5, 10 and 15 residues in two models of generalized Born implicit solvent (GB_{HCT} and GB_{OBC1}) to elucidate their structural and molecular properties as well as the relationship between these properties and the chain length. Such information would be beneficial for the selection of LFOs with appropriate lengths and properties for pharmaceutical and biological applications.

Methods

Structure preparation and minimization

The structures of LFO_5, LFO_{10} and LFO_{15} were constructed using the LEaP module in AMBER14 [20], and their atom types and force field parameters were assigned based on GLYCAM06j-1 [21]. Two implicit solvent models (GB_{HCT} and GB_{OBC1}) were used in the minimization and simulations of each system. All systems were minimized with 2500 steepest-descent minimization cycles and 2500 conjugate-gradient minimization cycles [22, 23].

Replica exchange molecular dynamics simulations

Sixteen replicas of each system were initially equilibrated for 500 ps to reach the desired temperature range from 262 to 802 K. REMD of all systems were performed using the SANDER module in AMBER14. Langevin dynamics with a collision frequency of 1 ps^{-1} were used to control the temperatures in all systems. Initial velocity of each system was reseeded by the random number generator [24]. A cut off of 999 Å was used to truncate nonbonded pairs, and the maximum distance of 999 Å between atom pairs was employed to compute the pairwise summation involved in the effective Born radii calculation. All bond-stretching freedoms associated with hydrogen were eliminated by SHAKE algorithm, allowing a time step of 0.002 ps [25]. Each replica was simulated for 100 ns and exchanged every 2 ps. The replicas at 298 K were employed for the analyses of the structural and molecular properties of LFOs with different chain lengths.

To measure the sizes of all systems, their average radii of gyration (ROG) were determined. To determine possible representative structures of LFOs of each chain length, K-means clustering algorithm, as implemented in MMTSB tool sets [26], was employed to cluster the structures from their 100 ns trajectories based on their structural similarities, calculated from their heavy-atom root-mean-square-deviation. To determine a reasonable representative of each cluster, a structure that is most similar to the average structure of all members of each cluster was chosen to be a "centroid;" i.e., a "centroid" is a structure with the lowest heavy-atom root-mean-square-deviation to the average structure. Based on their shapes, these "centroids" were further classified into helix-like, partial helix, zig-zag or random structures as major representative conformers. Helix-like structures were defined as conformations that had more than 1 helical turn, while partial helix structures were defined as conformations that had 1 helical turn. Zig-zag structures were defined as conformations that had zig-zag shapes. Random structures were defined as structures that were not classified as helix-like, partial helix or zig-zag structures.

To plot the free energy maps, various parameters were employed to characterize the structures of LFOs. Since helix-like conformations were observed with high frequencies in LFO_{10} and LFO_{15} and they tended to have similar values of upper-middle and lower-middle torsions, their upper-middle and lower-middle torsions were used to characterize the structures of LFO_{10} and LFO_{15}. Their upper-middle torsions were computed by measuring the torsion angles of the centers of masses (CM) of residues 5, 6, 7 and 8 (defined as $\chi_{6\text{-}7} = CM_5\text{-}CM_6\text{-}CM_7\text{-}CM_8$) and residues 3, 4, 5 and 6 (defined as $\chi_{4\text{-}5} = CM_3\text{-}CM_4\text{-}CM_5\text{-}CM_6$) for LFO_{15} and LFO_{10}, respectively. Their lower-middle torsions were computed by measuring the torsion angles of CMs of residues 8, 9, 10 and 11 (defined as $\chi_{9\text{-}10} = CM_8\text{-}CM_9\text{-}CM_{10}\text{-}CM_{11}$) and residues 6, 7, 8 and 9 (defined as $\chi_{7\text{-}8} = CM_6\text{-}CM_7\text{-}CM_8\text{-}CM_9$) for LFO_{15} and LFO_{10}, respectively (Fig. 1b, c). For LFO_5, the molecular angles and middle torsions were computed by measuring the angles and torsion angles of CMs of residues 1, 3 and 5 (defined as $\theta_a = CM_1\text{-}CM_3\text{-}CM_5$) and residues 2, 3, 4 and 5 (defined as $\chi_{3\text{-}4} = CM_2\text{-}CM_3\text{-}CM_4\text{-}CM_5$), respectively (Fig. 1d).

To measure conformational flexibilities, the occurrence frequencies of three dihedral angles between every two fructosyl residues, ω (C4-C5-C6-O6), ψ (C5-C6-O6-C2') and ϕ (C6-O6-C2'-O5') (Fig. 1e) were computed. To identify hydrogen bonds important for the formation of helix-like structures of LFO_{10} and LFO_{15}, the occurrence frequencies of hydrogen bonds were measured. Only the hydrogen bonds with the occurrence frequency of at least 1 % were used for further analysis.

Results and discussion

Reliability of REMD simulations

To determine whether the temperatures were optimally distributed and the number of replicas was sufficient, the acceptance ratios of replica exchange were calculated. The acceptance ratios of the simulations of LFO_{15} in the GB_{HCT} model were almost constant around 28 %, implying a free random walk in the replica (temperature) space (Additional file 1: Figure S1a). Moreover, a free random walk both in the replica space (Additional file 1: Figure S1b) and the temperature space (Additional file 1: Figure S1c) were also confirmed. Furthermore, the canonical probability distribution of the total potential energy at each temperature had sufficient overlap with those of neighbors (Additional file 1: Figure S1d). The results of the REMD simulations of LFO_{10} and LFO_5 in the GB_{HCT} model were also similar, and their average acceptance ratios were almost constant around 37 and 50 % for LFO_{10} and LFO_5, respectively. For the systems simulated in the GB_{OBC1} model, the results of REMD simulations were also similar to those simulated in the GB_{HCT} model, and their average acceptance ratios were almost constant around 28, 36 and 50 % for LFO_{15}, LFO_{10} and LFO_5, respectively. These results indicate good reliability of the REMD simulations of all systems.

Sizes of LFOs

The sizes of LFOs were determined by measuring their radii of gyration. Figure 2 shows that the trends of the radii of gyration of LFOs simulated in the GB_{HCT} model and those simulated in the GB_{OBC1} model are similar. The radii of gyration of LFOs tended to increase as their chain lengths increased from 5 to 15 residues. These results suggest the extension of the structures of LFOs as their chain lengths increase.

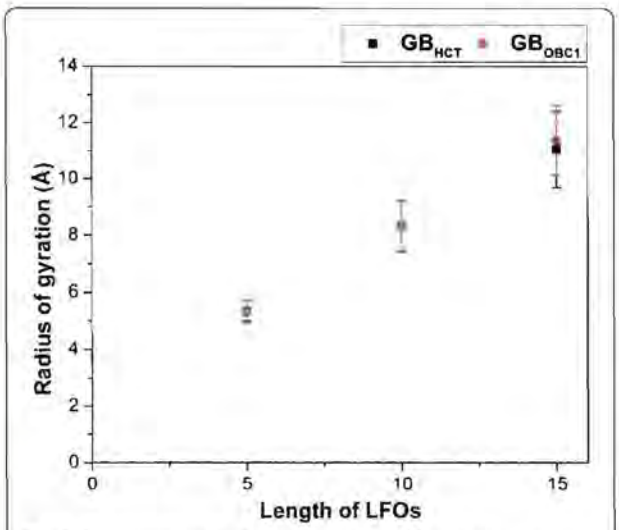

Fig. 2 The average radii of gyration calculated from the heavy atoms of LFOs simulated in GB_{HCT} (square) and GB_{OBC1} (dot) models

Conformations of LFO_{15}, LFO_{10} and LFO_5

Figure 3 shows the free-energy maps of LFO_{15}, LFO_{10} and LFO_5 as simulated in GB_{HTC} and GB_{OBC1} models as well as their major representative conformers and their population sizes from clustering analysis and centroid classification. For LFO_{15}, four major conformations such as helix-like (a), partial helix (b), zig-zag (c) and random (d) structures were observed after clustering analysis and centroid classification (Fig. 3a, b and Additional file 1: Figure S2 and Figure S5), and they were characterized by their upper-middle and lower-middle torsions ($\chi_{6\text{-}7}$ and $\chi_{9\text{-}10}$). Helix-like structures were found with the highest population of 54.1 and 63.2 % for those simulated in GB_{HCT} and GB_{OBC1} models, respectively. Helix-like structures took up conformations of left-handed 3-fold helices and tended to have their upper-middle and lower-middle torsions in the similar range of around 240–315°. The conformations with the second highest population were partial helix structures, and their population sizes were 33.9 and 22.3 % for systems simulated in GB_{HCT} and GB_{OBC1} models, respectively. The other two conformations were zig-zag and random structures. Zig-zag structures were found with the population sizes of 2.8 and 6.7 % for systems simulated in GB_{HCT} and GB_{OBC1} models, respectively. The population sizes of random structures simulated in GB_{HCT} and GB_{OBC1} models were 9.2 and 7.8 %, respectively.

Similar to the conformations of LFO_{15}, four major conformations such as helix-like (a), partial helix (b), zig-zag (c) and random (d) structures were found for LFO_{10} after clustering analysis and centroid classification (Fig. 3c, d and Additional file 1: Figure S3 and Figure S6). These conformations were characterized by their upper-middle and lower-middle torsions ($\chi_{4\text{-}5}$ and $\chi_{7\text{-}8}$). The conformation with the highest population sizes of 50.5 and 57.5 % was helix-like structures for those simulated in GB_{HCT} and GB_{OBC1} models, respectively. Partial helix structures occurred with the second highest population sizes of 34.5 and 25.4 % for those simulated in GB_{HCT} and GB_{OBC1} models, respectively. The population sizes of zig-zag structures were 6.8 and 8.7 % and those of random structures were 8.2 and 8.4 % for systems simulated in GB_{HCT} and GB_{OBC1} models, respectively.

For LFO_5, two major conformations such as partial helix (b) and random (d) structures were observed after clustering analysis and centroid classification, probably due to its shorter chain length as compared to those of

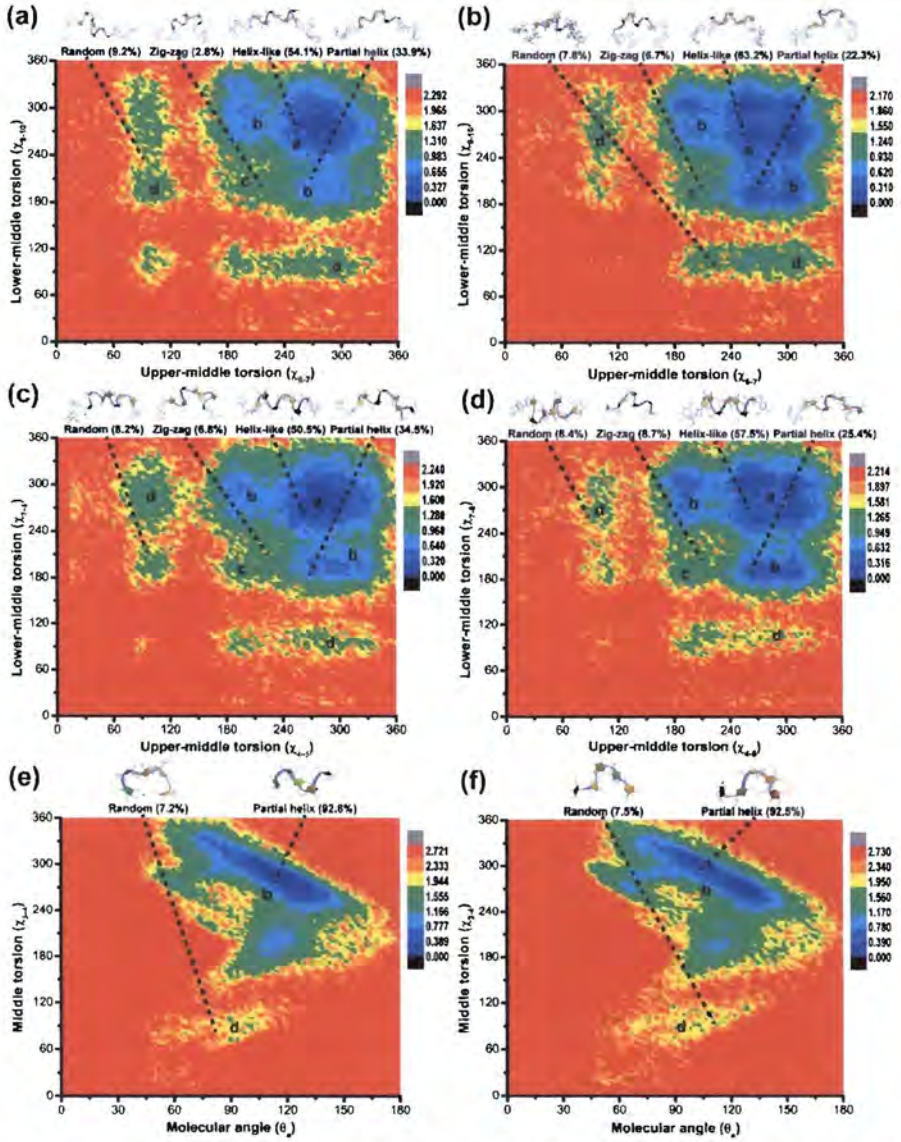

Fig. 3 The relative free energy (kcal/mol) maps of LFO_{15} (**a**), LFO_{10} (**c**) and LFO_5 (**e**) simulated in the GB_{HCT} model as well as those of LFO_{15} (**b**), LFO_{10} (**d**) and LFO_5 (**f**) simulated in the GB_{OBC1} model. The groups a, b, c and d are helix-like, partial helix, zig-zag and random structures. Their major representative conformers and populations are also shown

LFO_{10} and LFO_{15} (Fig. 3e, f and Additional file 1: Figure S4 and Figure S7). These conformations were characterized by their molecular angles (θ_a) and middle torsion (χ_{3-4}). Partial helix structures were observed with the population sizes of 92.8 and 92.5 % for those simulated in GB_{HCT} and GB_{OBC1} models, respectively. Random structures were also found with the population sizes of 7.2 and 7.5 % for those simulated in GB_{HCT} and GB_{OBC1} models, respectively.

Table 1 shows the populations of major representative conformers of LFO_{15}, LFO_{10} and LFO_5 simulated in GB_{HCT} and GB_{OBC1} models as determined from clustering analysis and centroid classification. As the chain length increased, the population of the helix-like structures tended to increase. These results may suggest that LFOs have tendencies to form helices as their chain lengths are extended.

Hydrogen bonds important for the formation of helix-like structures

To elucidate the hydrogen bonds important for the formation of helix-like structures, the occurrence

Table 1 The populations of major representative conformers of LFO_{15}, LFO_{10} and LFO_5 simulated in GB_{HCT} and GB_{OBC1} models as determined from clustering analysis and centroid classification

Solvent model	Major representative conformer	Population (%)		
		LFO_{15}	LFO_{10}	LFO_5
GB_{HCT}	Helix-like structure	51.4	50.5	-
	Partial helix structure	33.9	34.5	92.8
	Zig-zag structure	2.8	6.8	-
	Random structure	9.2	8.2	7.2
GB_{OBC1}	Helix-like structure	63.2	57.5	-
	Partial helix structure	22.3	25.4	92.5
	Zig-zag structure	6.7	8.7	-
	Random structure	7.8	8.4	7.5

frequencies of hydrogen bonds in helix-like structures of LFO_{15} and LFO_{10} with the occurrence frequencies of at least 1 % were analyzed. For the systems simulated in the GB_{HCT} model, the $O6_{(i)}$–$H3O_{(i+1)}$ hydrogen bonds (between residue i and i + 1) were found with the highest frequency, and their glycosidic oxygens acted as important hydrogen bond acceptors that interacted with the hydroxyl groups of C3 atoms of the furanose rings and probably helped stabilize the helix-like structures (Table 2 and Fig. 4). The hydrogen bonds with the second and third highest occurrence frequencies for both LFO_{15} and LFO_{10} were the $O1_{(i)}$–$H3O_{(i)}$ and $O5_{(i)}$–$H1O_{(i)}$ hydrogen bonds, which were the hydrogen bonds within the same residue (Table 2 and Fig. 4). The trends of the occurrence frequencies of the hydrogen bonds of LFO_{15} and LFO_{10} in the GB_{OBC1} model were also similar to those in the GB_{HCT} model (Table 2). These three hydrogen bonds ($O6_{(i)}$–$H3O_{(i+1)}$, $O1_{(i)}$–$H3O_{(i)}$ and $O5_{(i)}$–$H1O_{(i)}$ hydrogen bonds), especially the $O6_{(i)}$–$H3O_{(i+1)}$ hydrogen bond that was found with the highest frequency, are probably important for the formation of helix-like structures of LFO_{15} and LFO_{10} as their occurrence frequencies are higher than other hydrogen bonds.

Table 2 Occurrence frequencies of hydrogen bonds found in helix-liked structures of LFO_{15} and LFO_{10}

Solvent model	Residue that form a hydrogen bond	Type	Occurrence frequency[a] (%)	
			LFO_{15}	LFO_{10}
GB_{HCT}	i, i	$O1_{(i)}$–$H3O_{(i)}$	15.4	15.3
		$O5_{(i)}$–$H1O_{(i)}$	11.5	12.5
	i, (i + 1)	$O6_{(i)}$–$H3O_{(i+1)}$	65.0	60.2
GB_{OBC1}	i, i	$O1_{(i)}$–$H3O_{(i)}$	10.0	10.0
		$O5_{(i)}$–$H1O_{(i)}$	8.3	7.8
	i, (i + 1)	$O6_{(i)}$–$H3O_{(i+1)}$	37.5	34.8

[a]Only hydrogen bonds with the occurrence frequency of at least 7 % are shown

Conformational flexibilities

To investigate the conformational flexibilities of LFO_{15}, LFO_{10} and LFO_5, the occurrence frequencies of ω, ψ and ϕ of all glycosidic bonds were measured. For the systems simulated in the GB_{HCT} model, ψ and ϕ of all glycosidc linkages of all LFOs exhibited single major peaks around 173° and -63°, respectively (Fig. 5). However, ω was more flexible than ψ and ϕ as it exhibited one major peak and two minor peaks (Fig. 5). The results from the systems simulated in the GB_{OBC1} model were similar (Additional file 1: Figure S8); ω exhibited more peaks and was more flexible than ψ and ϕ. These results suggest that the flexibility of ω may be responsible for the conformational diversity of LFOs since this dihedral angle has more possibilities in rotating and changing the conformations of LFOs.

Conclusions

To elucidate the structural and molecular properties of LFOs as well as the relationship between these properties and their chain lengths, REMD were performed on systems of LFO_5, LFO_{10} and LFO_{15} in GB_{HCT} and GB_{OBC1} solvent models. We found that as the chain length increased, the radii of gyration tended to increase, suggesting the extension of the conformations as the chain length increases. After clustering analysis and centroid classifications, four major representative conformations (helix-like, partial helix, zig-zag and random structures) were found for LFO_{15} and LFO_{10}, while two conformations (partial helix and random structures) were identified for LFO_5. The free energy maps show that the four conformations of LFO_{15} and LFO_{10} were characterized by their upper-middle and lower-middle torsions, whereas the two conformations of LFO_5 were characterized by their molecular angles and middle torsions. As the chain length increased from 5 to 15 residues, the conformation populations of the helix-like structures tended to increase, suggesting the possible tendency of LFOs to form helices as their chain lengths are extended. Moreover, the $O6_{(i)}$–$H3O_{(i+1)}$ hydrogen bond was found with the highest frequency, suggesting its importance in helix formation of LFO_{15} and LFO_{10}. Furthermore, ω was found to be more flexible than ψ and ϕ and probably responsible for the conformational diversity of LFOs. This study gives important insights into the structural and molecular properties of LFOs; they tend to form helical structures as the chain length increases from 5 to 15 residues. Our findings may be useful in the selection of LFOs with appropriate chain lengths and structural properties for pharmaceutical and biological applications.

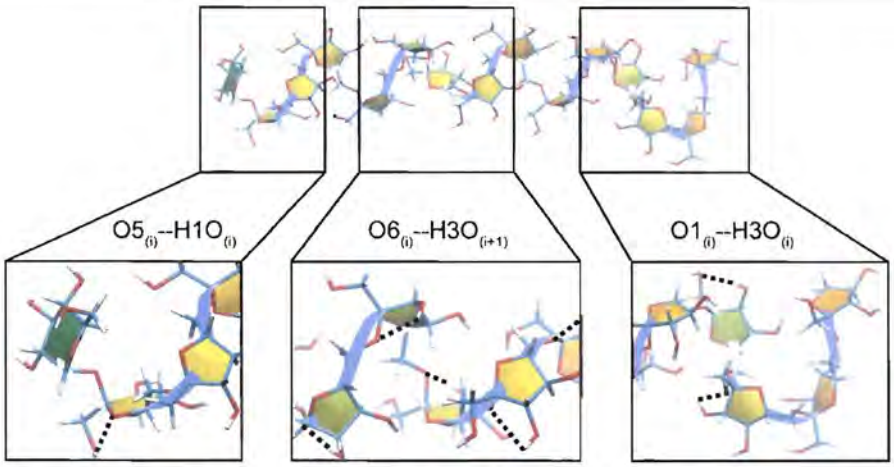

Fig. 4 Hydrogen bonds important for the formation of helix-like structures (LFO_{15} simulated in the GB_{HCT} model is shown as an example). Middle; the $O6_{(i)}$–$H3O_{(i+1)}$ hydrogen bond (occurrence frequency = 65.0 %). Right; the $O1_{(i)}$–$H3O_{(i)}$ hydrogen bond. (occurrence frequency = 15.4 %). Left; the $O5_{(i)}$–$H1O_{(i)}$ hydrogen bond (occurrence frequency = 11.5 %). Hydrogen bonds are represented as dash lines. The LFO chain and fructosyl units are represented as ribbon and filled yellow color representations, respectively

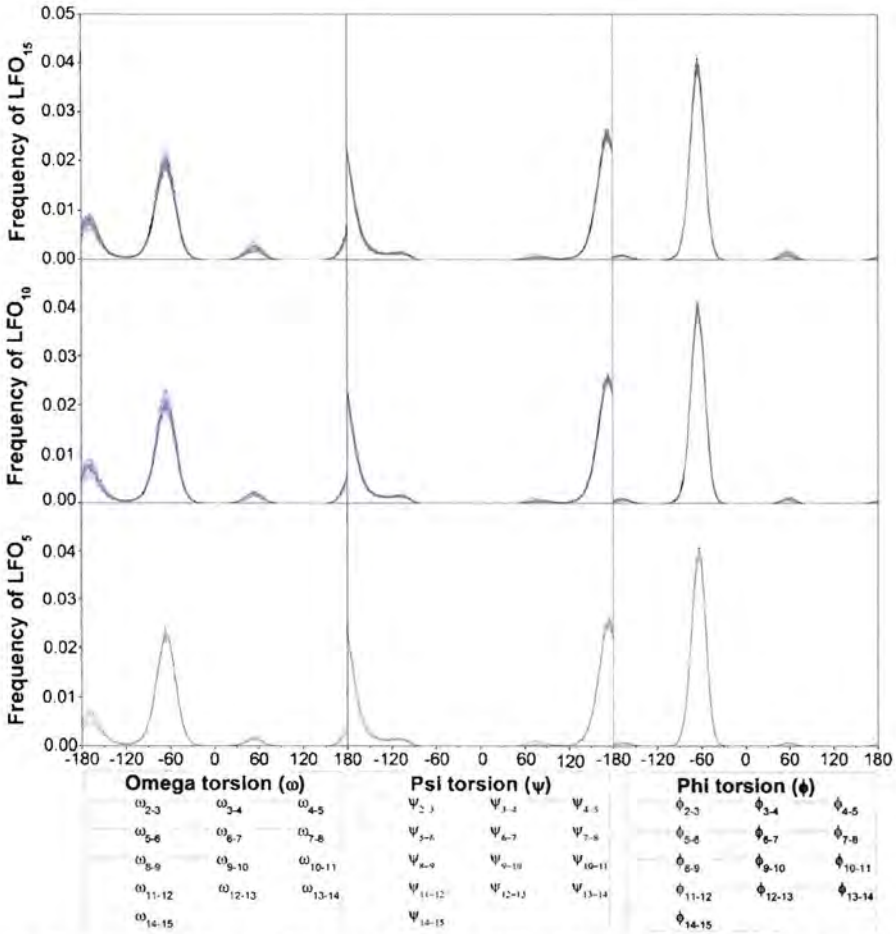

Fig. 5 The frequencies of the three dihedral angles of all glycosidic linkage of LFO_{15}, LFO_{10} and LFO_5 in the GB_{HCT} model. Each dihedral angle is shown in different color

Additional file

Additional file 1: Figure S1. (a) The acceptance ratio of replica exchange of the adjacent pairs of the simulations of LFO_{15} in the GB_{HCT} model. (b) Replica exchange at 298 K. (c) Time series of temperature exchange of three arbitrary chosen replicas 2 (*black*), 8 (*red*) and 16 (*blue*). (d) The canonical probability of the total potential energy of the systems at 16 temperatures simulated in the GB_{HCT} model. **Figure S2.** The "centroid" structure of each cluster of LFO_{15} simulated in the GB_{HCT} model. Their conformation types and populations are also shown. **Figure S3.** The "centroid" structure of each cluster of LFO_{10} simulated in the GB_{HCT} model. Their conformation types and populations are also shown. **Figure S4.** The "centroid" structure of each cluster of LFO_5 simulated in the GB_{HCT} model. Their conformation types and populations are also shown. **Figure S5.** The "centroid" structure of each cluster of LFO_{15} simulated in the GB_{OBC1} model. Their conformation types and populations are also shown. **Figure S6.** The "centroid" structure of each cluster of LFO_{10} simulated in the GB_{OBC1} model. Their conformation types and populations are also shown. **Figure S7.** The "centroid" structure of each cluster of LFO_5 simulated in the GB_{OBC1} model. Their conformation types and populations are also shown. **Figure S8.** The frequencies of the three dihedral angles of all glycosidic linkage of LFO_{15}, LFO_{10} and LFO_5 in the GB_{OBC1} model. Each dihedral angle is shown in different color. (DOCX 4740 kb)

Acknowledgment
We would like to thank Computational Chemistry Unit Cell (CCUC), Department of Chemistry, Chulalongkorn University for computer resources, helpful advice and discussion.

Funding
This study was funded by the Thailand Research Fund (TRF) [Grant no. TRG5880227]; Grants for Development of New Faculty Staff, Ratchadaphiseksomphot Endowment Fund, Chulalongkorn University [Grant no. GDNS 57-042-23-010 and GDNS 59-010-23-006]; Structural and Computational Biology Research Group, Special Task Force for Activating Research (STAR), Faculty of Science, Rachadaphiseksomphot Endowment Fund, Chulalongkorn University. This work was also partially supported by the Thailand Research Fund [Grant no. IRG 5780008]. PK was supported by the 100th Anniversary Chulalongkorn University Fund for Doctoral Scholarship. SC was partially supported by the Institute for the Promotion of Teaching Science and Technology (IPST) under the Research Fund for DPST Graduate with First Placement [Grant no. 07/2557]; Research Grant for New Scholar, Ratchadaphiseksomphot Endowment Fund, Chulalongkorn University [Grant no. RGN_2558_002_01_23]; and the Integrated Innovation Academic Center: Chulalongkorn University Centenary Academic Development Project. RP was partially supported by Rachadaphiseksomphot Endowment Fund Part of the "Strengthen CU's Researcher's Project.

Availability of data and materials
Data of the simulations are available upon request.

Authors' contributions
PK performed REMD, the data analysis and wrote the manuscript. RP conceived the study, performed the data analysis and revised the manuscript. SC conceived and designed the study, performed the data analysis, wrote and revised the manuscript. All authors read and approved the manuscript.

Competing interests
The authors declare that they have no competing interests.

Consent for publication
Not applicable.

Ethics approval and consent to participate
Not applicable.

Received: 3 June 2016 Accepted: 12 August 2016
Published online: 17 August 2016

References

1. Steinmetz M, Le Coq D, Aymerich S, et al. The DNA sequence of the gene for the secreted *Bacillus subtilis* enzyme levansucrase and its genetic control sites. Mol Gen Genet. 1985;200(2):220–8.
2. Goldman D, David N, Schwartz A, et al. Two Active Forms of *Zymomonas mobilis* Levansucrase: An ordered microfibril structure of the enzyme promotes levan polymerization. J Biol Chem. 2008;283(47):32209–17.
3. Kang HK, Seo MY, Seo ES, et al. Cloning and expression of levansucrase from *Leuconostoc mesenteroides* B-512 FMC in *Escherichia coli*. Biochim Biophys Acta. 2005;1727(1):5–15.
4. Dawes E, Ribbons D. Sucrose utilization by *Zymomonas mobilis*: formation of a levan. Biochem J. 1966;98:804–12.
5. Dogsa I, Brloznik M, Stopar D, et al. Exopolymer diversity and the role of levan in *Bacillus subtilis* biofilms. PLoS ONE. 2013;8(4):e62044.
6. Srikanth R, Reddy CHS, Siddartha G, et al. Review on production, characterization and applications of microbial levan. Carbohydr Polym. 2015;120:102–14.
7. Arvidson SA, Rinehart BT, Gadala-Maria F. Concentration regimes of solutions of levan polysaccharide from *Bacillus sp.* Carbohydr Polym. 2006; 65(2):144–9.
8. Han YW. Microbial levan. Adv Appl Microbiol. 1990;35(171–194):2
9. Gibson GR, Probert HM, Van Loo J, et al. Dietary modulation of the human colonic microbiota: updating the concept of prebiotics. Nutr Res Rev. 2004; 17(02):259–75.
10. Yamamoto Y, Takahashi Y, Kawano M, et al. In vitro digestibility and fermentability of levan and its hypocholesterolemic effects in rats. J Nutr Biochem. 1999;10(1):13–8.
11. Marx SP, Winkler S, Hartmeier W. Metabolization of β-(2, 6)-linked fructose-oligosaccharides by different bifidobacteria. FEMS Microbiol Lett. 2000;182(1):163–9.
12. Rairakhwada D, Pal A, Bhathena Z, et al. Dietary microbial levan enhances cellular non-specific immunity and survival of common carp (Cyprinus carpio) juveniles. Fish Shellfish Immunol. 2007;22(5):477–86.
13. Yoo S-H, Yoon EJ, Cha J, et al. Antitumor activity of levan polysaccharides from selected microorganisms. Int J Biol Macromolec. 2004;34(1):37–41.
14. Sugita Y, Okamoto Y. Replica-exchange molecular dynamics method for protein folding. Chem Phys Lett. 1999;314(1):141–51.
15. Earl DJ, Deem MW. Parallel tempering: Theory, applications, and new perspectives. Phys Chem Chem Phys. 2005;7(23):3910–6.
16. Re S, Miyashita N, Yamaguchi Y, et al. Structural diversity and changes in conformational equilibria of biantennary complex-type N-glycans in water revealed by replica-exchange molecular dynamics simulation. Biophys J. 2011;101(10):44–6.
17. Nishima W, Miyashita N, Yamaguchi Y, et al. Effect of bisecting GlcNAc and core fucosylation on conformational properties of biantennary complex-type N-glycans in solution. J Phys Chem B. 2012;116(29):8504–12.
18. Jo S, Qi Y, Im W. Preferred conformations of N-glycan core pentasaccharide in solution and in glycoproteins. Glycobiology. 2016;26(1):19–29.
19. Shen T, Langan P, French AD, et al. Conformational flexibility of soluble cellulose oligomers: chain length and temperature dependence. J Am Chem Soc. 2009;131(41):14786–94.
20. Case D, Babin V, Berryman J, et al. AMBER 14. 2014. University of California, San Francisco.
21. Kirschner KN, Yongye AB, Tschampel SM, et al. GLYCAM06: a generalizable biomolecular force field. Carbohydrates. J Comput Chem. 2008;29(4):622–55.
22. Hawkins GD, Cramer CJ, Truhlar DG. Parametrized models of aqueous free energies of solvation based on pairwise descreening of solute atomic charges from a dielectric medium. J Phys Chem. 1996;100(51):19824–39.
23. Onufriev A, Bashford D, Case DA. Modification of the generalized Born model suitable for macromolecules. J Phys Chem B. 2000;104(15):3712–20.
24. Cerutti DS, Duke R, Freddolino PL, et al. A vulnerability in popular molecular dynamics packages concerning Langevin and Andersen dynamics. J Chem Theory Comput. 2008;4(10):1669–80.
25. Ryckaert J-P, Ciccotti G, Berendsen HJ. Numerical integration of the cartesian equations of motion of a system with constraints: molecular dynamics of n-alkanes. J Comput Phys. 1977;23(3):327–41.
26. Feig M, Karanicolas J, Brooks CL. MMTSB Tool Set: enhanced sampling and multiscale modeling methods for applications in structural biology. J Mol Graph Model. 2004;22(5):377–95.